International Journal of Pharmaceutics 641 (2023) 123093

Contents lists available at ScienceDirect

International Journal of Pharmaceutics

journal homepage: www.elsevier.com/locate/ijpharm

3D printed macroporous scaffolds of PCL and inulin-g-P(D,L)LA for bone tissue engineering applications

Carmela Tommasino [a,b], Giulia Auriemma [a,*], Carla Sardo [a], Carmen Alvarez-Lorenzo [c], Emilia Garofalo [d], Silvana Morello [a], Giovanni Falcone [a], Rita P. Aquino [a]

[a] Department of Pharmacy, University of Salerno, Via Giovanni Paolo II 132, I-84084 Fisciano (SA), Italy
[b] PhD Program in Drug Discovery and Development, University of Salerno, Via Giovanni Paolo II 132, I-84084 Fisciano, Italy
[c] Departamento de Farmacología, Farmacia y Tecnología Farmacéutica, I+D Farma (GI-1645), Facultad de Farmacia, Instituto de Materiales (IMATUS), Health Research Institute of Santiago de Compostela (IDIS), Universidade de Santiago de Compostela, Santiago de Compostela 15782, Spain
[d] Department of Industrial Engineering, University of Salerno, Via Giovanni Paolo II 132, I-84084 Fisciano (SA), Italy

ARTICLE INFO

Keywords:
Inulin-g-poly(D,L)lactide
Poly(ε-caprolactone)
Hybrid biodegradable material
Fused filament fabrication
3D printing
Hybrid 3D printed scaffolds
Bone tissue engineering

ABSTRACT

Bone repair and tissue-engineering (BTE) approaches require novel biomaterials to produce scaffolds with required structural and biological characteristics and enhanced performances with respect to those currently available. In this study, PCL/INU-PLA hybrid biomaterial was prepared by blending of the aliphatic polyester poly(ε-caprolactone) (PCL) with the amphiphilic graft copolymer Inulin-g-poly(D,L)lactide (INU-PLA) synthetized from biodegradable inulin (INU) and poly(lactic acid) (PLA). The hybrid material was suitable to be processed using fused filament fabrication 3D printing (FFF-3DP) technique rendering macroporous scaffolds. PCL and INU-PLA were firstly blended as thin films through solvent-casting method, and then extruded by hot melt extrusion (HME) in form of filaments processable by FFF-3DP. The physicochemical characterization of the hybrid new material showed high homogeneity, improved surface wettability/hydrophilicity as compared to PCL alone, and right thermal properties for FFF process. The 3D printed scaffolds exhibited dimensional and structural parameters very close to those of the digital model, and mechanical performances compatible with the human trabecular bone. In addition, in comparison to PCL, hybrid scaffolds showed an enhancement of surface properties, swelling ability, and in vitro biodegradation rate. In vitro biocompatibility screening through hemolysis assay, LDH cytotoxicity test on human fibroblasts, CCK-8 cell viability, and osteogenic activity (ALP evaluation) assays on human mesenchymal stem cells showed favorable results.

1. Introduction

Tissue engineered (TE) scaffolds have become a strategic approach to repair or even replace injured tissues, overcoming certain critical limitations of autografts (donor site morbidity and limited quantity), allografts (high failure rate and risk for infections) and xenografts (zoonoses) (Wang et al., 2019). Most of injuries involve bone tissues (Fu et al., 2011), and as bone plays critical functions in the human body such as homeostasis of minerals, locomotion, load-bearing capacity and protection of the internal organs (Grabowski, 2015), there is a special need for suitable bone grafts.

Several critical aspects should be considered when designing a bone scaffold. First, biomaterials with suitable features to support cell adhesion and proliferation (e.g., with adequate chemical composition and good surface properties such as roughness and wettability) need to be carefully selected. Moreover, the physical structure of the scaffold in

Abbreviations: 3DP, 3D-printing; BTE, bone tissue engineering; CDI, carbonyl diimidazole; DSC, Differential scanning calorimetry; DMF, dimethylformamide; EtOEt, diethylether; FFF, fused filament fabrication; FT-IR, Fourier-Transform Infrared Spectroscopy; GPC, Gel permeation chromatography; HME, hot melt extrusion; hMSC, human mesenchymal stem cells; INU, inulin; INU-PLA, Inulin-g-poly(D,L)lactide; LDH, lactate dehydrogenase; M_n, number-average molecular weight; M_w, weight-average molecular weight; NMR, Nuclear Magnetic Resonance; PBS, phosphate buffered saline; PCL, poly(ε-caprolactone); PDI, polydispersity index; PLA, poly(lactic acid); pNPP, p-nitrophenyl phosphate; Ra, Arithmetical mean roughness; Rq, Root mean square roughness; SD, standard deviation; SEM, scanning electron microscopy; T_c, Crystallization temperature; TE, tissue engineered; TEA, triethylamine; THF, Tetrahydrofuran; T_m, melting temperature; UHR-SEM, ultra-high resolution scanning electron microscope; ΔH_c, crystallization enthalpy; ΔH_m, melting enthalpy.

* Corresponding author at: University of Salerno, Via Giovanni Paolo II 132, I-84084 Fisciano (SA), Italy.
E-mail address: gauriemma@unisa.it (G. Auriemma).

https://doi.org/10.1016/j.ijpharm.2023.123093
Received 15 February 2023; Received in revised form 26 May 2023; Accepted 27 May 2023
Available online 31 May 2023

terms of pore size, macro-porosity, and tortuosity of 3D architecture must mimic the native bone tissue (Chocholata et al., 2019). Only with a rational design considering all such features, the produced scaffolds could really meet clinical needs, and be readily translatable (Zhang et al., 2019).

Additive manufacturing and particularly 3D printing (3DP) techniques are offering new opportunities and solutions not achievable through less-controlled conventional fabrication techniques such as freeze-drying, solvent casting and particulate leaching or gas foaming (Eltom et al., 2019). Thanks to the ability to produce, in a highly controlled way, 3D objects with complex shape, geometry, and architecture starting from a customizable digital model, 3DP may allow the production of personalized scaffolds based on specific patient needs (Montero et al., 2021). Among different 3D printing techniques, Fused Filament Fabrication (FFF) is the most versatile and cost effective tool for the controllable and reproducible production of scaffolds with 3D macroporous architecture (Kim and Kim, 2015; Schätzlein et al., 2022), useful for the treatment of large bone defects (Wang et al., 2019). While FFF-3DP technology is being increasingly refined, biomaterials suitable for printing remain very limited (Kutikov et al., 2015). The choice is mainly constrained to synthetic biodegradable polyesters such as poly (lactic acid) (PLA) (Schätzlein et al., 2022), poly(glycolic acid) (Boland et al., 2001), poly(lactide-co-glycolide) (Li et al., 2002) and poly (ε-caprolactone) (PCL) (Dwivedi et al., 2020). Such polymers have good and varied elastic, mechanical and chemical properties, and a foreseeable, even if slow, degradation (Malberg et al., 2011). However, their affinity for cell is generally poor as a consequence of their hydrophobicity and lack of surface cell-recognition sites (Dwivedi et al., 2020). Such issues can be overcome simply by combining materials of a different nature (Kutikov et al., 2015; Verdú et al., 2002), and polymer blending has emerged as top effective method for providing new, desirable hybrid biomaterials for particular applications (Alhosseini et al., 2012; Hamlehkhan et al., 2012). Many studies have shown that blending aliphatic polyesters with synthetic (Wang et al., 2021a), semisynthetic (Van Hoorick et al., 2020) and natural polymers (Kim and Kim, 2015), or also with non-polymeric materials such as bioglasses (Schätzlein et al., 2022) and bioceramics (Wang et al., 2021b), may improve cell adhesion, and the degradation rate of the blended polymeric systems.

The aim of the present work was to develop a novel PCL-based hybrid biomaterial for the manufacturing of customizable 3D printed bone macroporous scaffolds by blending with a graft copolymer derived from inulin. We wanted to challenge the question whether hybridization of PCL with the amphiphilic, amorphous, and thermoplastic graft copolymer Inulin-g-poly(D,L)lactide (INU-PLA) (Sardo et al., 2022) may produce a high-performance polymeric blend able to maintain the PCL printability while enhancing its critical physicochemical properties. Particularly, the key point was the improvement of the poor hydrophilicity/wettability which strongly determine its biological performances, as well as its slow biodegradation. It should be noted that inulin has been used for microextrusion 3D printing of fat analogs (Shahbazi et al., 2021; Wen et al., 2021), but it has not been tested so far as component of bone scaffolds despite dietary inulin has been demonstrated to play a key role in bone health (Meyer and Stasse-Wolthuis, 2006). Inulin is a natural, renewable polysaccharide, consisting of D-fructose units linked by β (2–1) glycosidic linkages, easily extractable from different vegetable sources, biocompatible and biodegradable (Mensink et al., 2015). Orally administered inulin has been shown to significantly enhance the bone mineral content of the cortical bone in both appendicular and peripheral sites and reduce bone sorption (Nzeusseu et al., 2006). Also, studies in osteoblastic cell lines have evidenced that certain inulin varieties promote proliferation, differentiation, and mineralization (Yan et al., 2019). Inulin has also been tested for wound healing sponges as a cross-linking agent of collagen and as an antioxidant agent (Kalirajan et al., 2022). In the last decade, inulin has been highly explored as a polymer backbone to construct advanced functional materials for biomedical applications due to the high number of hydroxyls of the dangling fructose units which allow its functionalization as well as its structural flexibility (Sardo et al., 2016; Tripodo and Mandracchia, 2019). INU-PLA was already proposed as alternative to PEG-PLA to produce nano-drug delivery systems for antineoplastic agents (Sardo et al., 2022). This copolymer showed amphiphilic properties, which make it soluble in a wider variety of aqueous and organic media compared to isolated blocks and, therefore, miscible with different substances. It also exhibited thermoplastic behavior, an aspect that significantly increases its processability.

To produce the hybrid material, PCL and INU-PLA were firstly blended as thin films through solvent-casting method, and then filaments suitable for FFF-3DP were obtained by HME. The PCL/INU-PLA blends in form of extruded filaments were then deeply investigated in terms of physicochemical properties, homogeneity, wettability, and processability by FFF-3DP. The resulting 3D printed PCL/INU-PLA scaffolds were characterized in terms of dimension, porosity, 3D architecture, surface topography. Studies also included evaluation of thermal properties, mechanical performances, swelling ability, and in vitro hydrolytic biodegradation (both long-term and accelerated). In vitro biological assays were conducted to evaluate the biocompatibility of the hybrid 3D printed scaffolds by hemolysis test, cytotoxicity on human fibroblasts (LDH), and finally cell viability (CCK-8 test) and osteogenic activity (ALP) on human mesenchymal stem cells (hMSCs).

2. Materials and methods

2.1. Materials

Polycaprolactone (PCL) filament (Facilan™ Ortho Filament) M_w = 104 kDa, M_n = 77 kDa (calculated by GPC) was purchased from 3D4Makers (3D4Makers, Paris, France). Materials for inulin-graft-poly-D,L-lactide (INU-PLA) synthesis were supplied as described below: inulin from Dahlia tubers (INU, Mw ≈ 5000 Da), triethylamine (TEA), and carbonyl diimidazole (CDI), diethylether (EtOEt) were purchased from Merck. Poly(D,L-lactide) acid endcap (PDLLA, M_n: 5,000–10,000) was obtained by PolySciTech (Division of Akina, West Lafayette, IN). INU was dried at 70 °C overnight in an oven and cooled down under vacuum over P_2O_5 prior to be dissolved for reaction. All other chemical reagents and solvents were supplied from Sigma Aldrich (St. Louis MO, USA) and used as received.

2.2. General procedure for the synthesis and characterization of Inulin-graft-poly-D,L-lactide (INU-PLA)

INU-PLA was synthetized as previously reported (Sardo et al., 2022). Briefly, INU (100 mg, $61.67 \cdot 10^{-2}$ mmol of fructose repeating units) was dissolved in 1.2 mL of anhydrous dimethylformamide (DMF) at room temperature (4 h). TEA (0.172 mL, 2 eq/mmol INU repeating units) was then added and the mixture stirred at 40 °C for few minutes. A solution of activated PDLLA (0.12 eq/mmol INU repeating units in 3 mL of anhydrous DMF, previously activated with 2 eq of CDI for 4 h at 40 °C), was then added, and the mixture was reacted at 40 °C for 67 h. The solid pure product was obtained by precipitation and washings with a mixture of EtOEt/Acetone 85:15 for two times and then dried under vacuum. The spectroscopic characterization is in accordance with previous findings. ^{1}H NMR (400 MHz, DMSO-d_6, ppm) δ 5.54 – 5.40 (m, 1H, PLA-C***H***(CH_3)C(O)OCH_2-INU, 5.35 (s, 1H, ***HO***-CH(CH_3)C(O)O-PLA), 5.25 – 5.14 (m, 1H, PLA-C***H***(CH_3)C(O)O-PLA), 5.14 (d, J = 5.5 Hz, 1H, CH(4)O***H*** fructose), 4.69 (d, J = 6.3 Hz, 1H, CH(3)O***H*** fructose), 4.59 (t, J = 4.7 Hz, 1H, CH_2(6)O***H*** fructose), 4.20 (dd, J = 13.0, 6.1 Hz, 1H, HOC***H***(CH_3)C(O)O-PLA), 4.06 (t, J = 7.2 Hz, 1H, C***H***(4)OH fructose), 3.80 (d, J = 4.7 Hz, 1H, C***H***(3)OH fructose), 3.74 – 3.38 (m, 5H, C***H$_2$***(6)C***H***(5) + C***H$_2$***(1) INU), 1.46 (q, J = 5.5 Hz, 3H, PLA-CH(C***H$_3$***)C(O)O-PLA), 1.35 – 1.20 (m, 6H, HOCH(***CH_3***)C(O)O-PLA-CH(***CH_3***)C(O)O-INU). FT-IR (ATR, cm^{-1}) 3312, 2940, 3887, 1749, 1647, 1456, 1381, 1327, 1260, 1192, 1129,

Table 1
Composition and main characteristics of PCL/INU-PLA extruded filaments: polymeric blend composition, INU-PLA/PCL mass ratio, HME process yield, diameter, and water contact angle values (n = 3, mean values and, in parenthesis, standard deviations).

Lab Extruded Filament name	Polymeric blend composition	INU-PLA/PCL mass ratio	Yield (%)	Diameter (mm)	Water contact angle
//	PCL**	//	//	2.85 (0.01)	82.27 (1.32)
Fil1	PCL/INU-PLA 2.5 wt%	0.0256	84.17	2.65 (0.09)	75.60 (1.12)
Fil2	PCL/INU-PLA 5.0 wt%	0.0526	83.57	2.83 (0.05)	71.00 (0.85)
Fil3	PCL/INU-PLA 10.0 wt%	0.1111	89.11	2.74 (0.10)	69.69 (1.69)

** Commercial PCL.

1082, 1027, 988, 934, 871, 819. $DD_{mol\%}$8.32 $M_{n\ NMR}$ 25430 Da $M_{w\ GPC}$22700 Da PDI 2.12.

2.3. Fabrication of PCL/INU-PLA films

PCL/INU-PLA blend films were prepared using a solvent-casting method. INU-PLA (2.5, 5.0 or 10.0 wt%) was solubilized in DMF (2 mL). DMF (14 mL) and INU-PLA solution were added to PCL (7.8, 7.6 or 7.2 g, respectively) at 70° C. The mixture was sonicated and vortexed until the complete dispersion of the PCL, then it was casted into a glass Petri dish (diameter 140 mm), washed in deionized water to allow the removal of DMF and then left under a fume hood with nitrogen flow to ensure complete evaporation of the solvents. The resulting film (thickness around 200 μm) was then cut into small pieces and stored in controlled humidity conditions (over P_2O_5) until its use.

As control, films of PCL blended with Inulin ($Fil3_I$) and of PCL, Inulin and P(D,L)LA ($Fil3_{I+P}$) were also produced, using the same general procedure.

2.4. Filament manufacturing by hot melt extrusion

Pellets deriving from each casted film (about 8 g) were extruded using a single-screw filament extruder (Noztek Touch HT, Noztek, England) equipped with a pre-heater band (T_2) at the end of the mixing zone and a second heating chamber (T_1) before the nozzle. For an optimal extrusion process the instrument was set at the working temperatures of 70 °C (T_2) and 65 °C (T_1) and a rotational speed of 40 rpm, and it was equipped with a nozzle having a diameter of 3.0 mm.

An Electronic Digital Caliper 6″ (Toolsnow, China) was utilized in measuring the diameter for all extruded filaments, where measurements were taken up to two decimal points. The diameter was calculated by averaging at least 10 measurements and was expressed as mean ± standard deviation (SD).

The yield of the extrusion process was calculated using the following equation:

$$Yield\% = \frac{g\ \ of\ \ extruded\ \ filament}{g\ \ of\ \ pellet} \cdot 100 \quad (1)$$

Filament homogeneity was evaluated by ^{1}H NMR. For each extruded filament, two fragments were taken (the ends).

2.5. Water contact angle

Surface wettability of the developed materials was evaluated by measuring the static water contact angle. To homogenize surfaces of all tested samples, the extruded filaments were melted on a plate at 80 °C for obtaining circular rigid discs (thickness around 400 μm and diameter of about 2 cm) macroscopically smooth and flat (Bruyas et al., 2018). A drop of double-distilled water (10 μL) (Huhtamäki et al., 2018) was placed on the disc, a photograph was taken 30 s after drop deposition with a single-lens reflex camera (Canon EOS 600D; parameters: f-stop: f/6.3, shutter speed: 1/5 s, ISO 200) to obtain macroscopic images of the deposited drops and the contact angle was measured using ImageJ® software (Wayne Rasband, National Institute of Health, Bethesda, MD, USA). Contact angle was calculated as the average of 3 measurements performed at different locations of the disks and it was expressed as mean ± SD.

2.6. Nuclear Magnetic Resonance Spectroscopy (NMR)

^{1}H NMR spectra were recorded using a Bruker Avance III spectrometer operating at 400 MHz. DMSO-d_6, $CDCl_3$, DMF-d7, were used for INU-PLA, PCL and their blends respectively. Samples were prepared

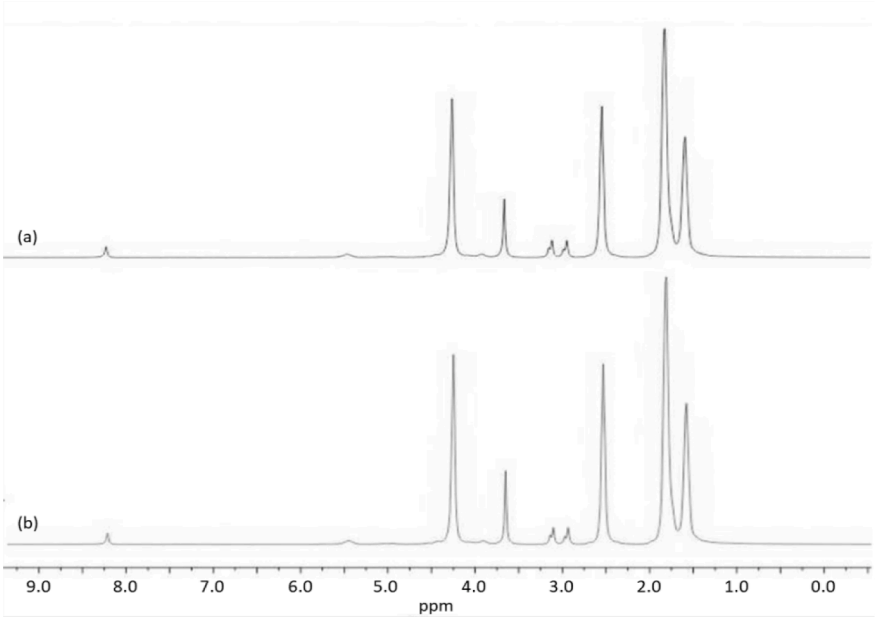

Fig. 1. ^{1}H NMR spectra of the first **(a)** and the last **(b)** extruded part of Fil3 recorded in DMF-d7.

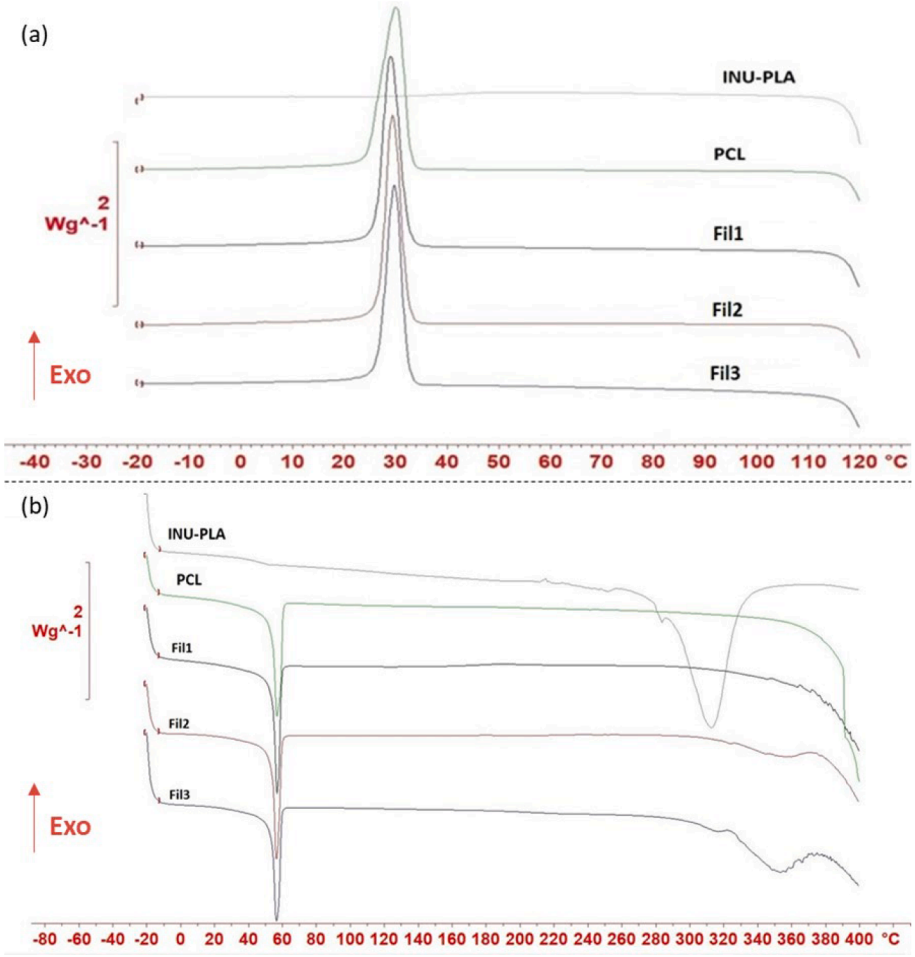

Fig. 2. Comparative plot of DSC curves of raw materials (PCL** and INU-PLA) and PCL/INU-PLA filaments with three different INU-PLA contents: cooling cycle (a) and second heating cycle (b) ** Commercial PCL.

dissolving 10 mg of the solid in 0.6 mL of deuterated solvent.

^{1}H NMR of PCL in blend with Inulin (PCL/I) was recorded both in DMF-d7 and in hot D_2O to isolate signals for PCL and INU, respectively. Specifically, samples in D_2O were prepared using the following extraction procedure: 10 mg of the solid was dissolved in 300 μL of Tetrahydrofuran (THF). Then, extract inulin from PCL matrix, 600 μL of hot (60 °C) D_2O were added. The mixture was stirred at room temperature for 40 min under N_2 flow until the complete evaporation of THF. After that, it was brought to 60 °C and stirred for another hour. The supernatant was subjected to NMR analysis. Residual solvent signals were used as reference, according with Fulmer et al. (Fulmer et al., 2010).

2.7. Fourier-transform infrared spectroscopy (FT-IR)

FT-IR spectra were recorded on the pure solid samples using an ATR single reflection sampling module on a Frontier FT-IR spectrometer (Perkin Elmer, USA). To ensure good contact between sample and crystal, samples in the form of discs were used. Discs were obtained by melting a filament fragment on a heating plate at 60 °C. 64 scans were collected in a wavenumber range of 4000–600 cm^{-1}.

2.8. Gel permeation chromatography (GPC)

The GPC system used consisted of a pump (LC-20AD, Shimadzu, Kyoto, Japan), a degassing unit (DGU-20A3R, Shimadzu, Kyoto, Japan) a forced air oven, three in serie GPC styrene–divinylbenzene copolymer gel fixed pore columns (10^3 Å, 10^4 Å and 10^5 Å, Phenogel, from Phenomenex srl, Italy) preceded by a guard column and a refractive index detector (Refractive Index Detector-10A, Shimadzu, Kyoto, Japan). GPC conditions were as follows: 2.5 mg/mL as sample concentration, 100 μL of injection volume, 1 mL/min flow rate. The detector cell of RID was kept at 40 °C. The elution solvent was pure THF. Samples were filtered on PTFE 0.45 μm syringe filters before injection. Data were acquired by the Lab Solutions Lite software (Shimadzu, Kyoto, Japan). Detailed information about processing and calibration are reported in Figure S3.

2.9. Differential scanning calorimetry (DSC)

All measurements were made in non-hermetic aluminum crucible (40 μL) in a Mettler Toledo 822e instrument. The sample amount was exactly weighed around 3 mg. Thermograms were obtained after the following cycles were applied: 1) heating from 25 to 120 °C, 10 K/min; 2) isotherm at 120 °C for 2 min; 3) cooling from 120 to −20 °C, 10 K/min; 4) heating from −20 to 300 °C, 10 K/min. During measurements, the sample cell was purged with nitrogen at a flow rate between 60 and 70 mL/min.

Crystallization temperature (T_c), melting temperature (T_m), melting enthalpy (ΔH_m) and crystallization enthalpy (ΔH_c) were measured. Crystallinity % was estimated from the following equation:

$$Crystallinity\ (\%) = \frac{\Delta H_m}{w\hat{A}\cdot\Delta H_{m100}}\cdot 100 \quad (2)$$

where ΔH_m is the melting enthalpy, ΔH_{m100} is the melting enthalpy of

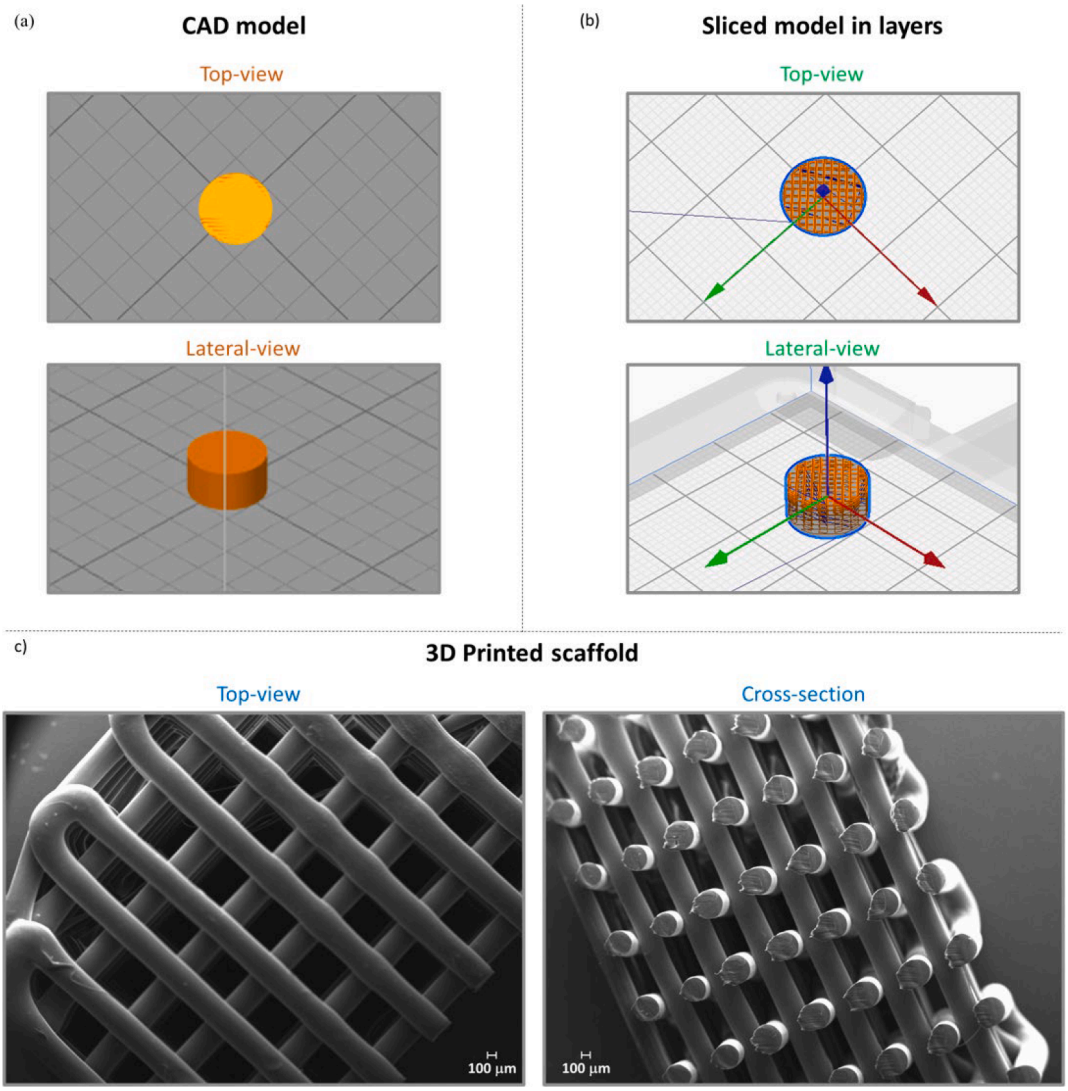

Fig. 3. (a) CAD design obtained using Rhinoceros 5 (cylinder, 10 mm diameter; 5 mm height); (b) Sliced model obtained via Cura 3.2.1 3D (14 layers; layer height = 0.35 mm and 0°- 90° patterns); (c) SEM micrographs of a PCL scaffold prepared using the optimized slicing and printing parameters (0.40 mm nozzle Ø, 85 °C extrusion temperature, 40 °C build plate temperature, 5 mm/s printing speed) (image on the left represents scaffold top-view and on the right its cross-section).

Table 2
Characteristics of PCL/INU-PLA scaffolds: weight, diameter, thickness, and porosity (n = 3, mean values and, in parenthesis, standard deviations).

Scaffold	Weight (mg)	Diameter (mm)	Thickness (mm)	Porosity (%)
S	143.72 (5.11)	9.61 (0.17)	4.65 (0.11)	62.83 (4.11)
S1	147.92 (10.28)	9.60 (0.18)	4.76 (0.09)	62.16 (1.67)
S2	142.29 (7.63)	9.25 (0.12)	4.70 (0.07)	65.86 (2.52)
S3	139.35 (9.81)	9.31 (0.11)	4.68 (0.07)	62.05 (2.82)

100% crystalline PCL ($\Delta H_{m100} = 139.5$ J/g), w is the weight fraction of the polymeric portion in the blend (Mi et al., 2014).

2.10. 3D printing of porous scaffolds

All the extruded filaments were fed into the 3D printing equipment and printed in the form of 3D porous scaffolds, using the FFF 3D printer Ultimaker3 (Ultimaker, Netherlands).

First, cylindrical CAD models of the scaffolds were drawn using Rhinoceros 5 (Robert McNeel & Associates, McNeel Europe) and exported as stereolithographic files (.stl). Graphical designs were then processed by the slicing software Cura 3.2.1 (Ultimaker, Netherlands), creating the g-code file used by the printer. Main slicing and printing parameters are described below.

Object configuration: 10 mm diameter, 5 mm height, 0.6 mm pore size, 0.35 mm layer height, and 14 total layers. The infill pattern was linear and infill density was 38%. Printer was equipped with a nozzle of 0.40 mm in diameter and set at extrusion temperature of 85 °C, build plate temperature of 40 °C and print speed of 5 mm/s.

2.11. Porosity

The porosity of the scaffolds was measured using a liquid displacement method (Loh and Choong, 2013). The scaffold was placed in a cylinder with a known volume (3 mL) of absolute ethanol. The cylinder was subjected to 5 series of compression-decompression, using a vacuum pump, to force the liquid into the scaffold pores. In the end, the impregnated scaffold was removed from the solution.

The porosity was calculated using the following equation:

$$Porosity\ (\%) = \frac{V_1 - V_3}{V_2 - V_3} 100 \quad (3)$$

where V_1 is the known volume of ethanol that was used to submerge the scaffold, V_2 is the volume of the liquid and liquid-impregnated scaffold,

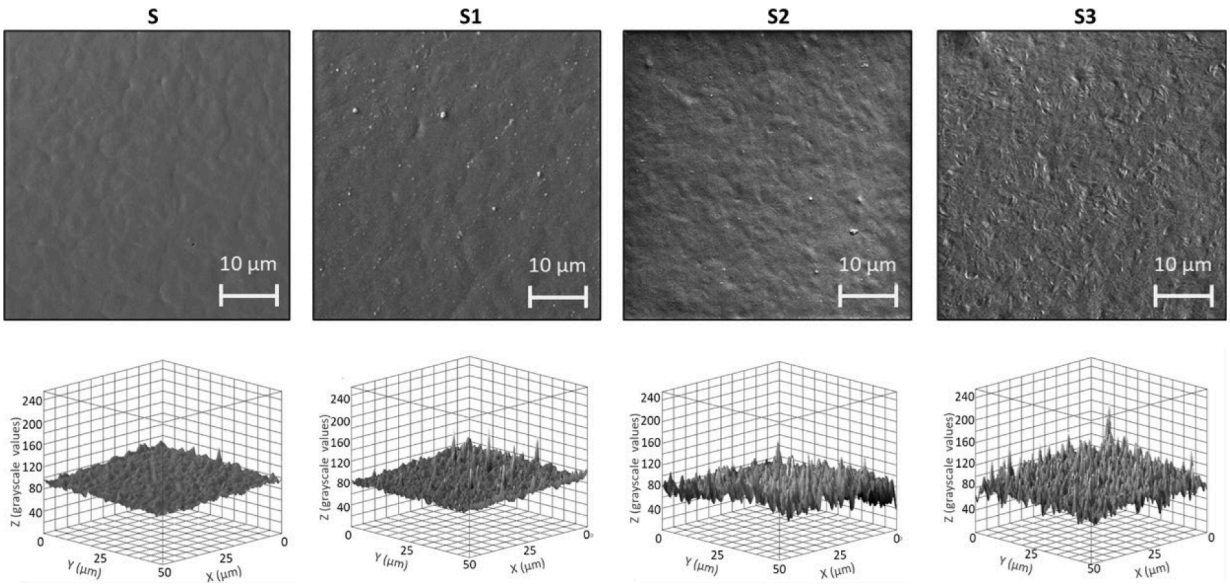

Fig. 4. Representative SEM images of the surface of S and S1, S2 and S3 hybrid scaffolds (top) and 3D surface reconstruction by ImageJ from SEM images (down).

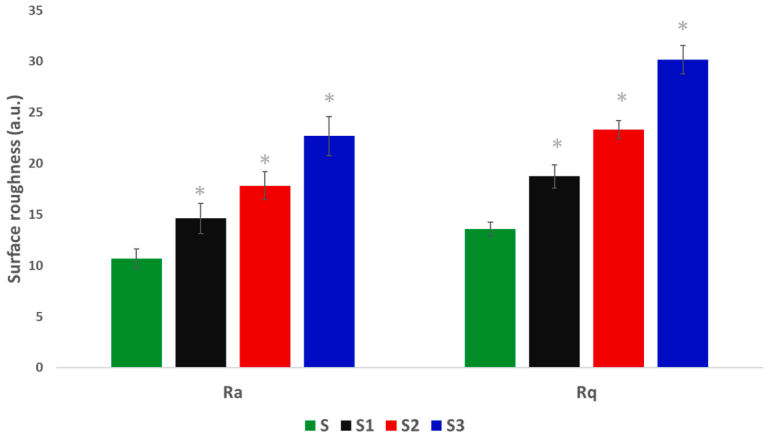

Fig. 5. Root mean square roughness (Rq) and arithmetical mean roughness (Ra) values of PCL and PCL/INU-PLA scaffolds. Asterisks mark significant differences vs S (Student's T test, $p < 0.05$).

and V_3 is the remaining liquid volume after scaffold removal.

2.12. Dimensional, morphological, and topographical analysis

Scaffold diameter and thickness were measured with an Electronic Digital Caliper 6″ (Toolsnow, China). Each measure was performed in triplicate and results were expressed in terms of mean ± SD. Scaffold morphology and 3D architecture were examined using scanning electron microscopy (SEM) using Carl Zeiss EVO MA 10 microscope with a secondary electron detector (Carl Zeiss SMT Ltd., Cambridge, UK). Scaffolds were placed onto metal plates and 200–400 Å-thick gold layer was sputter-coated on the samples with a LEICA EMSCD005 before viewing. The analysis was conducted at 20 KeV. Some scaffolds were fractured using a scalpel to obtain cross-section views.

Scaffold surface topography was analyzed by an ultra-high resolution scanning electron microscope (UHR-SEM) Tescan Solaris (Tescan Orsay Holding, Czech Republic) after sample metallization with a 200–400 Å-thick gold layer. To obtain surface information, the analysis was conducted at 5 KeV, and all sample micrographs were acquired at the same Field of View (50 µm) and magnification (4.19 kx). The surface roughness of the scaffold struts was evaluated analyzing the acquired SEM images through the SurfCharJ 1 q plug-in (Chinga et al., 2007) of ImageJ® software (Wayne Rasband, National Institute of Health, Bethesda, MD, USA). Images were converted to 32-bit and scaled prior to analysis (Wu et al., 2016). Root mean square roughness (Rq) and arithmetical mean roughness (Ra) values were calculated with the selected plug-in, ticking the options: level surface, local roughness analysis, and perform gradient analysis (https://www.gcsca.net/IJ/SurfCharJ.html) (Gadelmawla et al., 2002). Surface roughness evaluation was conducted on 50 µm × 50 µm areas (so that strut curvature would not contribute to the measurements). Tilt controls were also conducted of overlapping measurements to confirm that features remain unaltered (Kumar et al., 2012). The analysis was carried out on 3 different struts per scaffold type and data (roughness parameters) were expressed as mean ± SD.

In addition, 3D Interactive surface plot plug-in of ImageJ® software was used to show representative 3D reconstructions of the scaffold surfaces (Wu et al., 2016).

2.13. Mechanical tests

The compressive moduli and compressive strength of all scaffolds (n = 3/group) were measured in a mechanical testing bench (CMT6000, MST, Pechino, Cina; 1 kN load cell) and calculated using the mechanical

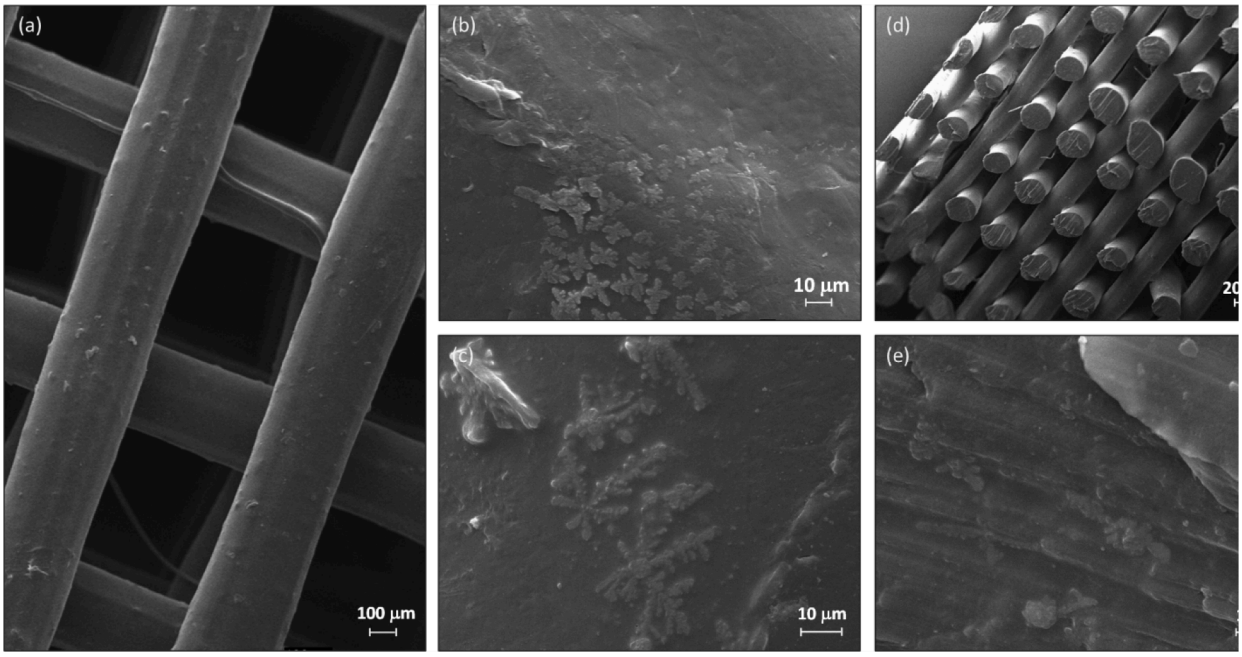

Fig. 6. SEM micrographs of S3 scaffolds prepared using FFF 3D printing: (a) Top-view; (b) and (c) strut topography at different magnification (2500X and 3000X, respectively); (d) cross-section; (e) strut cross-section magnification (3000X).

Table 3
Thermal parameters of PCL and PCL/INU-PLA scaffolds obtained by DSC analysis. The crystallization temperature (T_c) and enthalpy (ΔH_c) were measured during the cooling cycle, while the melting temperature (T_m) and enthalpy (ΔH_m) were calculated during the second heating cycle.

Sample	T_m(°C)			ΔH_m (J/g)	T_c(°C)			ΔH_c (J/g)	Cristallinity %
	Onset	Endset	Peak		Onset	Endset	Peak		
S	54.20(0.15)	59.75(0.27)	56.63(0.19)	69.51(1.93)	33.95(0.72)	27.71(0.55)	31.14(0.46)	61.09 (1.81)	49.83 (1.38)
S1	53.96(0.15)	59.01(0.56)	56.41(0.02)	66.82(1.35)	32.43(0.65)	27.06(0.46)	29.86(0.40)	63.96 (0.24)	49.13 (1.00)
S2	53.81(0.32)	59.53(0.48)	56.52(0.08)	67.25(1.57)	33.31(1.39)	26.21(0.29)	29.85(0.70)	62.32 (3.73)	50.74 (1.18)
S3	54.06(0.04)	59.38(0.28)	56.45(0.03)	61.79(1.36)	32.86(0.13)	27.04(0.17)	30.31(0.09)	61.62 (1.97)	49.11 (1.08)

data analysis package included in the manufacturer's software. Scaffolds were compressed perpendicularly to their larger surface at a crosshead speed of 1 mm/min (after an initial 30 s pre-load of 25 N) up to 20% strain. Stress–strain curves were calculated from the load vs. displacement data using the initial external dimensions of each sample.

The compressive modulus was estimated using the slope of the linear portion of the stress–strain curve. Compressive strength was estimated by a 0.2% offset to the stress–strain curve (Bittner et al., 2019). Scaffolds were stored for 90 days in phosphate buffered saline (PBS) pH 7.4 at 37 °C and then re-evaluated regarding mechanical properties.

2.14. Swelling ability

Swelling ability of 3D printed scaffolds was evaluated by monitoring: 1) fluid uptake percentage over time in PBS at 37 °C, and 2) changes in scaffold strut width after 48 h of incubation in PBS.

More in detail, scaffolds were accurately weighed using a MX5 Mettler Toledo microbalance, immersed in PBS 0.1 M, pH 7.4 (Kim et al., 2018) containing 0.05% w/v sodium azide (NaN_3) to prevent microbe growth and incubated at 37 °C under stirring (110 rpm) using an Orbital Shaker (SKI 4, Argolab, Italy). At different time points (1, 2, 3, 7, 14 and 21 days), samples were removed from the medium, blotted dry to remove excess medium and added into a centrifuge tube. After centrifugation at 500 rpm for 3 min, the weight of scaffolds was recorded again. Fluid uptake (%) was calculated using the following equation (Zimmerling et al., 2021):

$$Fluid\ uptake\ (\%) = \frac{W_t - W_0}{W_0} \cdot 100 \quad (4)$$

where W_t is scaffold wet mass at selected time point after centrifugation, W_0 is scaffold initial mass.

To evaluate changes in scaffold strut width, samples at t0 and t48 h were analyzed by optical microscopy (Alphaphot-2 YS2, Nikon) at magnification 4X and microscopy images were processed through ImageJ® software (Wayne Rasband, National Institute of Health, Bethesda, MD, USA) (Kutikov et al., 2015). For each tested scaffold, strut width was calculated as the average of 5 measurements performed on different places. All the experiments were performed in triplicate, and results were expressed as mean ± SD.

2.15. In vitro degradation

The scaffolds were weighed precisely, submerged in individual tubes with PBS, pH = 7.4 containing 0.05% w/v sodium azide (NaN_3) to prevent microbe growth (Bazgir et al., 2021) and incubated at 37 °C under stirring (110 rpm), using an Orbital Shaker (SKI 4, Argolab, Italy). At certain time intervals (50, 90, 180 days), scaffolds were removed, rinsed thoroughly with deionized water and freeze-dried.

The percent weight loss of the scaffolds was calculated as follows (Lam et al., 2009):

$$Weight\ loss\ (\%) = \frac{W_0 - W_{dry}}{W_0} \cdot 100 \quad (5)$$

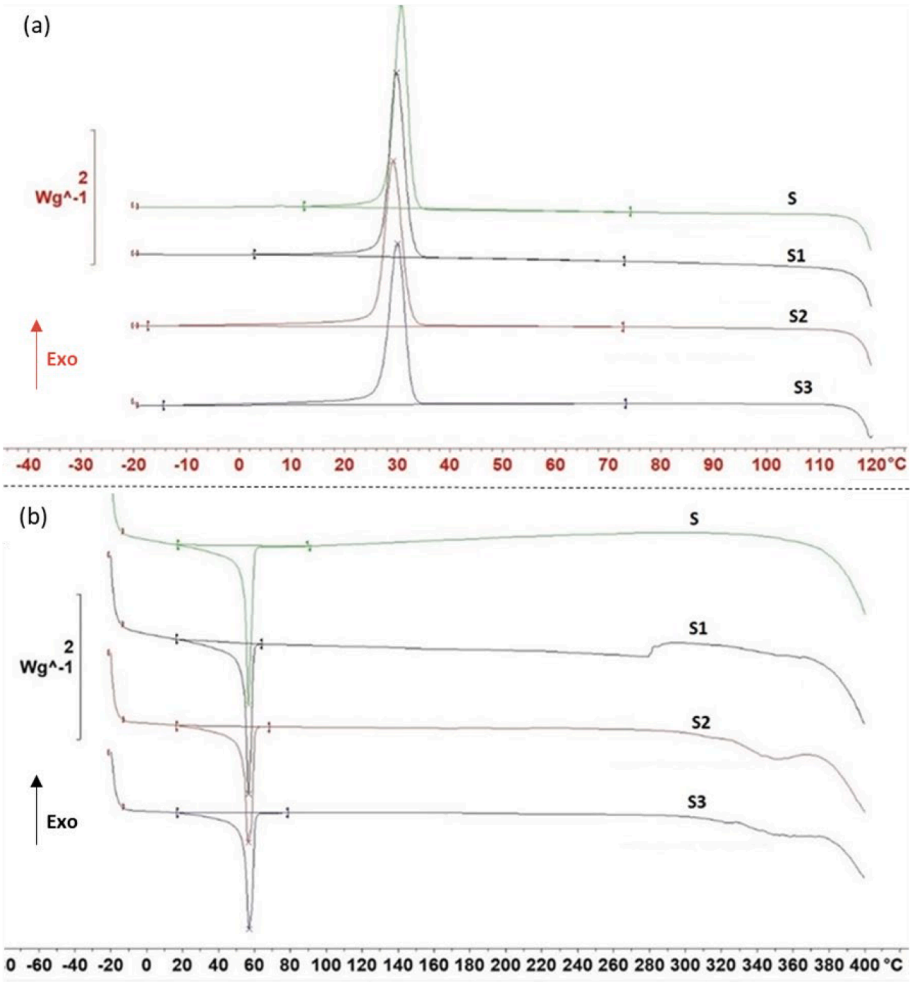

Fig. 7. Comparative plot of DSC curves of PCL and PCL/INU-PLA scaffolds with three different INU-PLA contents: cooling cycle **(a)** and second heating cycle **(b)**.

The number-average (M_n) and weight-average (M_w) molecular weights and the polydispersity index (PDI: M_w/M_n) of the scaffolds were determined using a GPC system, as previously reported.

The degradation properties of scaffolds were also evaluated using an in vitro enzymatic degradation accelerated model. Procedure from Vyas et al. (Vyas et al., 2021) was followed with slight modification. Briefly, scaffolds were weighed, sterilized by soaking in absolute ethanol for few seconds and then dried in a fume hood to allow the ethanol to completely evaporate. Each sample was transferred in a test tube with 2 mL of 0.1 M PBS (pH = 7.4) containing 0.5 mg/mL of Amano Lipase PS from Pseudomonas cepacia (Sigma Aldrich) and incubated at 37 °C under stirring (110 rpm) using an Orbital Shaker (SKI 4, Argolab, Italy). The lipase and PBS solution were changed every day to ensure enzyme activity. At certain time intervals (24, 48, 72, 96 h), scaffolds were removed, rinsed thoroughly with deionized water and freeze-dried. The dried samples were re-weighed at room temperature (20 °C) and the weight loss of each sample was expressed as a percentage of the original weight. Each experiment was performed in triplicate and the results were expressed as mean ± SD. Some samples were also analyzed by UHR-SEM in the conditions above described.

2.16. In vitro hemolysis test

Procedure from Xiang et al. (Xiang et al., 2018) was followed to determine the percentage of he molysis. Blood was collected from healthy volunteer in citrated tubes. Anticoagulated blood was diluted (4 mL blood in 5 mL saline) and used within 24 h. Scaffolds were placed into clean 15 mL centrifuge tubes together with 5 mL saline and pre-incubated for 30 min at 37 °C in an orbital shaker (60 rpm). 100 μL of diluted anticoagulated blood were then added into each tube and samples were incubated at 37 °C in an orbital shaker (100 rpm). After 60 min, tubes were centrifuged at 2000 rpm for 5 min and the supernatant read for absorbance at 545 nm. A blank of 5 mL saline added with 100 μL of diluted blood was used as a negative control (NC) while 5 mL double distilled water was added with 100 μL of diluted blood was used to obtain the 100% lysis (PC).

The hemolysis percentage was evaluated by the following equation:

$$Hemolysis(\%) = \frac{Abs_{scaffold} - Abs_{NC}}{Abs_{PC} - Abs_{NC}} \cdot 100 \quad (6)$$

Where $Abs_{scaffold}$ is the absorbance of tested samples; Abs_{NC} and Abs_{PC} are the absorbance of the negative and positive control, respectively. Hemolysis percentage was calculated by the mean of three measures for each scaffold.

2.17. LDH assay

In vitro cytotoxicity of 3D printed scaffolds was evaluated using human fibroblasts (MRC-5 - CCL-171, ATCC) and applying LDH assay. Cells were cultured in αMEM (EuroClone S.p.a, with Earle's Salts, L-Glutamine, without Sodium Pyruvate), supplemented with heat inactivated FBS (10%) and penicillin/streptomycin (1%) and grown at 37 °C/5% CO_2. For cell seeding, previously sterilized scaffolds (by soaking in absolute ethanol for few seconds and then allowing the ethanol to completely evaporate) were placed in 24-well-plates, then seeded with

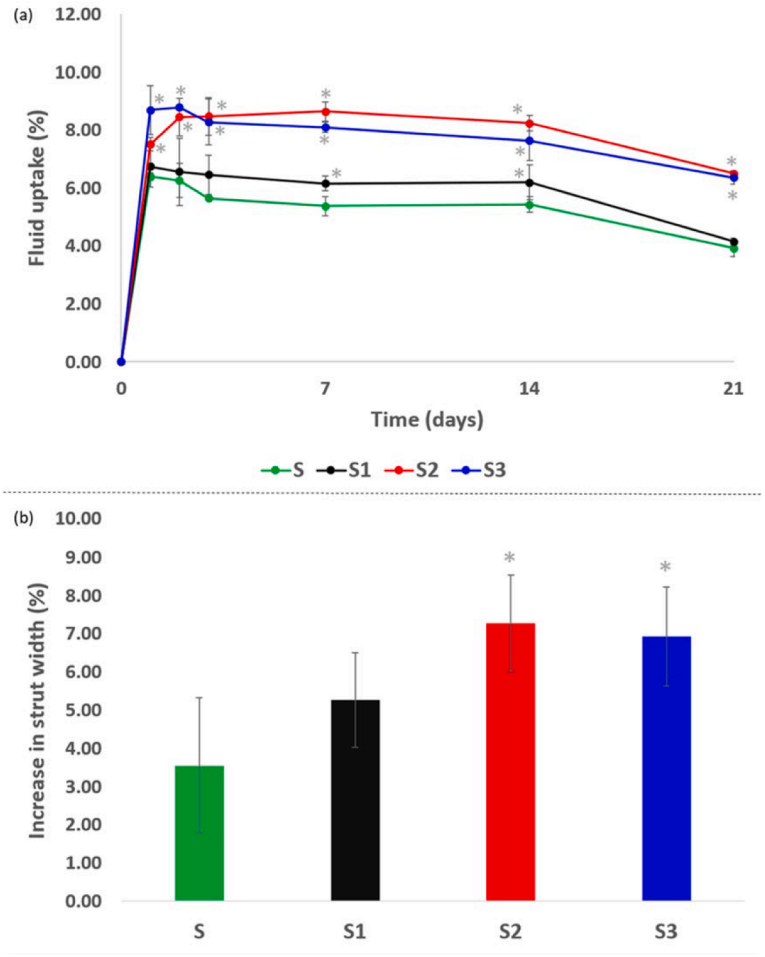

Fig. 8. Swelling behavior of PCL and PCL/INU-PLA scaffolds in PBS, pH 7.4 at 37 °C: (a) fluid uptake % over time and (b) changes in scaffold strut width after 48 h. Asterisks mark significant differences vs S (Student's T test, $p < 0.05$).

1 mL of culture medium containing 20000 cells and incubated for 48 h at 37 °C/5% CO_2. The cells in the wells without scaffolds were treated as control. The negative control required to determine the LDH activity spontaneously released from untreated normal cells, and the positive control to determine the maximum releasable LDH activity in the cells. After the incubation for 48 h at 37 °C/5% CO_2, the cells were treated with 1X TRITON provided in the Cytotoxicity Detection KitPlus (LDH, Roche). Aliquots of medium (100 µL) were taken and mixed with the reaction medium (100 µL) provided with the Cytotoxicity Detection KitPlus (LDH, Roche). The plates were incubated for 10 min at 15–25 °C protected from light. The absorbance at 490 nm was immediately measured with spectrophotometer (Titertek Multiskan MCC/340). The experiments were carried out in triplicate and cytotoxicity was calculated as follows (Babaie and Bhaduri, 2018):

$$Cytotoxicity(\%) = \frac{Abs_{exp} - Abs_{negative\ \ control}}{Abs_{positive\ \ control} - Abs_{negative\ \ control}} \cdot 100 \quad (7)$$

2.18. CCK-8 assay

Cell viability was carried out using human adipose-derived mesenchymal stem cells (hMSCs) (PCS-500–011, ATCC, USA). Cells were passaged in MEM-α medium supplemented with fetal bovine serum (10%), L-glutamine (1%) and antibiotics (penicillin–streptomycin; 1%). At 80% confluence, cells were trypsinized, counted using a hemocytometer and seeded on the scaffolds as follows. Scaffolds were immersed in ethanol, then washed three times with PBS, and incubated in 5 mL of FBS overnight. On the following day, scaffolds were placed individually in well of a 24-well plate and seeded with 500 µL of hMSC suspension with a concentration of 100000 cells/mL. In order to promote the homogeneous attachment of the cells on the scaffolds, the well plates were placed in a rotary seeding plate (5 rpm) for 1 h. Then, 500 µL of culture medium were added to each well, and the plates were incubated for 12 days at 37 °C and 5% CO_2. Culture medium was replaced every other day. At 3, 7 and 12 days, cell viability was quantitatively evaluated using a Cell Counting kit-8 (CCK-8; Dojindo, Japan) following the instructions provided by the manufacturer. Briefly, culture medium was replaced for 1 mL of CCK-8 working solution (10% v/v CCK-8 stock solution in culture medium) and incubated for 3 h at 37 °C. Finally, absorbance was recorded at 570 nm using a UV Bio-Rad Model 680 microplate reader (Bio-Rad Laboratories; Hercules CA, USA). Results were expressed as percentage of viability and compared to the PCL control scaffolds (S).

2.19. Confocal microscopy

hMSC morphology and density on the scaffold surface were evaluated using DAPI/Phalloidin staining. Briefly, cells were seeded on the scaffolds as explained in the previous paragraph and cultured for 3, 7 and 12 days at 37 °C and 5% CO_2. Then, culture medium was removed, and cells were washed with PBS, fixed with paraformaldehyde (4% w/v) for 10 min and then, washed again with PBS to remove non-adherent cells. Cells were permeabilized using 0.01% w/v Triton in PBS pH 7.4 during 5 min and washed again with PBS. F-actin was stained with Alexa Fluor 488-Phalloidin dye (0.16 µM in PBS) and incubated for 20 min in darkness. Then, scaffolds were washed again with PBS and a 1 µg/mL

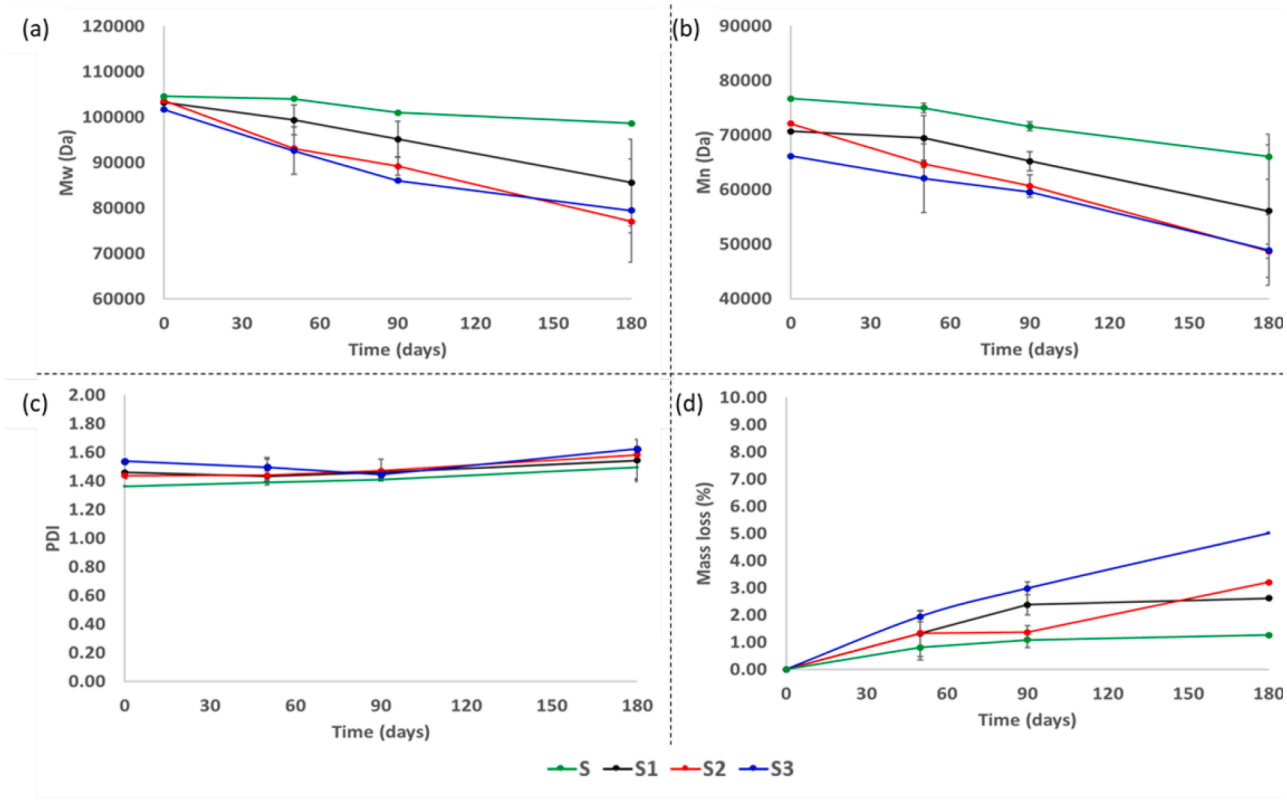

Fig. 9. Scaffold in vitro hydrolytic degradation profile over 180 days, in PBS, pH 7.4 at 37 °C: (a) Weight-average molecular weight (M_w), (b) Number-average molecular weight (M_n), (c) Polydispersity index, (d) Mass loss (%).

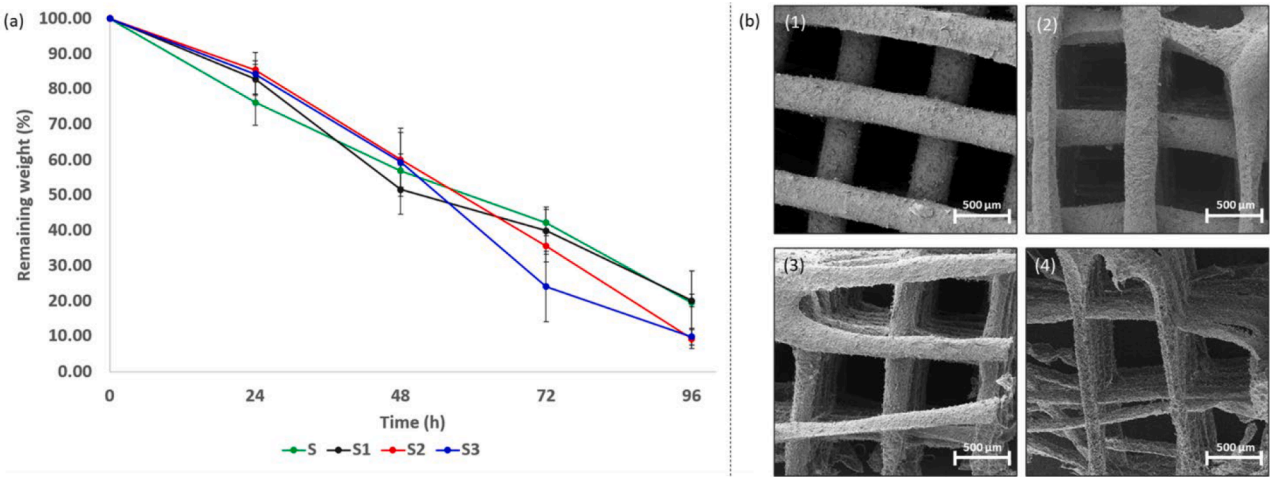

Fig. 10. Degradation of scaffolds in accelerated conditions: Panel (a): In vitro enzymatic degradation profiles. Panel (b): SEM micrographs of a S3 scaffold after (1) 24, (2) 48, (3) 72 and (4) 96 h, at magnification 120X.

DAPI solution was added to each sample and incubated for 3 min. Finally, scaffolds were washed in PBS and observed using a confocal microscope Leica Stellaris 8 (Leica, Germany).

2.20. ALP activity

hMSCs were seeded on the scaffolds as previously reported. After seeding, culture medium was replaced for osteogenic differentiation medium (MEM-α medium supplemented with 10% v/v FBS, 10 mM β-glycerol-2-phosphate, 10 nM dexamethasone, 50 mg/mL ascorbic acid, 1% v/v L-glutamine, and 1% v/v penicillin/streptomycin). After 3, 7 and 14 days of culture, medium was removed, and scaffolds were washed thrice with PBS. Then, 1 mL of sterile-filtered ultrapure water was added to each well and frozen at −80 °C. Samples were submitted to three freeze–thaw cycles followed by ultrasonication to lyse cells. The amount of DNA present on each scaffold was evaluated using a Quant-iT PicoGreen dsDNA Assay Kit (Molecular Probes, Eugene, OR) following manufacturer's protocol. Briefly, cell lysates or DNA standard were placed into the well of an opaque 96-well plate and incubated with the Quant-iT™ PicoGreen™ dsDNA Reagent working solution for 5 min at room temperature protected from light. Fluorescence was then measured at an excitation and emission wavelengths of 485 and 530 nm,

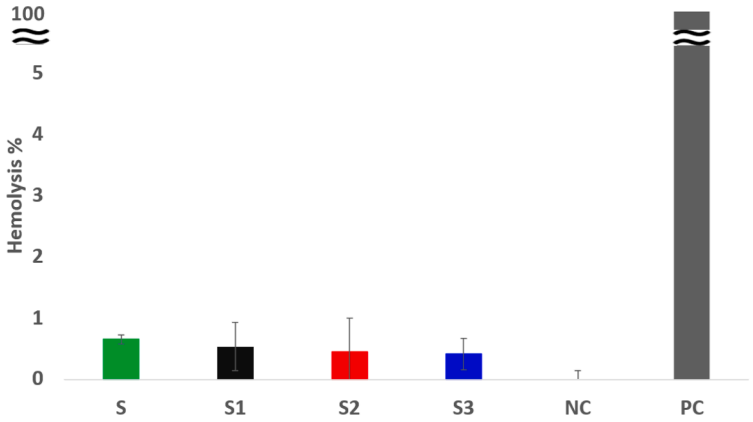

Fig. 11. Percentages of hemolysis after contact of the developed scaffolds with blood. NC, blank negative control: 5 mL saline added with 100 μL of diluted blood. PC, positive control 100% lysis: 5 mL double distilled water added with 100 μL of diluted blood.

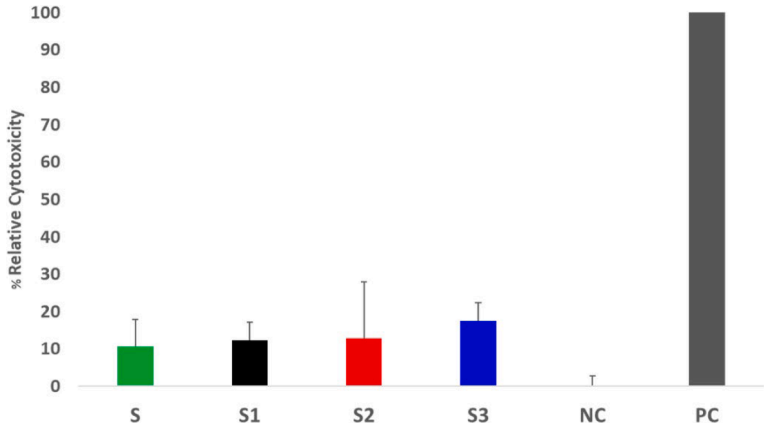

Fig. 12. Percentages of LDH released from human fibroblasts after 48 h direct contact with the developed scaffolds. NC, negative control: untreated cells. PC, positive control: maximum LDH release.

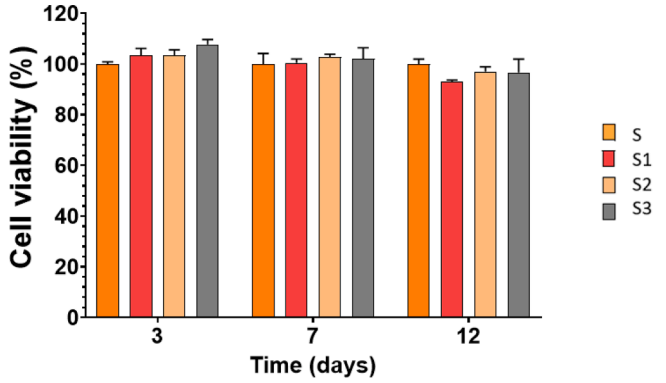

Fig. 13. Viability of hMSCs seeded on the PCL-based scaffolds after 3, 7 and 12 days of culture. Data are expressed as mean ± SD.

respectively, using a Fluostar Optima fluorescence microplate reader (BMG LabTech GmbH; Ortenberg, Germany). The level of alkaline Phoshatase (ALP), an early marker of osteogenic differentiation of hMSCs, was determined using a colorimetric assay kit (Alkaline Phosphatase Activity Assay; Abcam, Cambridge, MA), according to the instructions from the manufacturer. The cell lysatess, collected as before described, were incubated with a 5 mM p-nitrophenyl phosphate (pNPP) solution for 60 min. Finally, absorbance was measured at 405 nm using a microplate reader. ALP activity for each sample was calculated from a pNPP standard curve. Results were normalized by DNA content as measured by the PicoGreen assay.

2.21. Statistical analysis

Data are presented using mean ± SD. Statistical analyses were performed using Student's T test method. Differences were considered significant for $p < 0.05$, as labeled in figures by the * symbol.

3. Results and discussion

3.1. Polymeric blend preparation and characterization

Three different hybrid PCL/INU-PLA polymeric blends containing INU-PLA at 2.5, 5.0, and 10.0 wt% were designed (Table 1). To avoid low uniformity issues and maximize the homogeneity of each composition, mixtures were obtained in forms of films by using solvent-casting method and then cut into pellets, as described in the experimental section. As controls, two PCL blended films containing inulin ($Fil3_I$) and physical mixture of inulin and P(D,L)LA ($Fil3_{I+P}$) were also produced.

All polymeric blends in forms of pellets were successfully extruded into filaments using a single-screw filament extruder with process yields up to 90%. The extruded filaments were then characterized in terms of appearance, surface morphology, size, chemical composition and component interactions, homogeneity, wettability, thermal properties, and, finally, processability by FFF-3DP technology.

All filaments exhibited good surface properties without defects (e.g.,

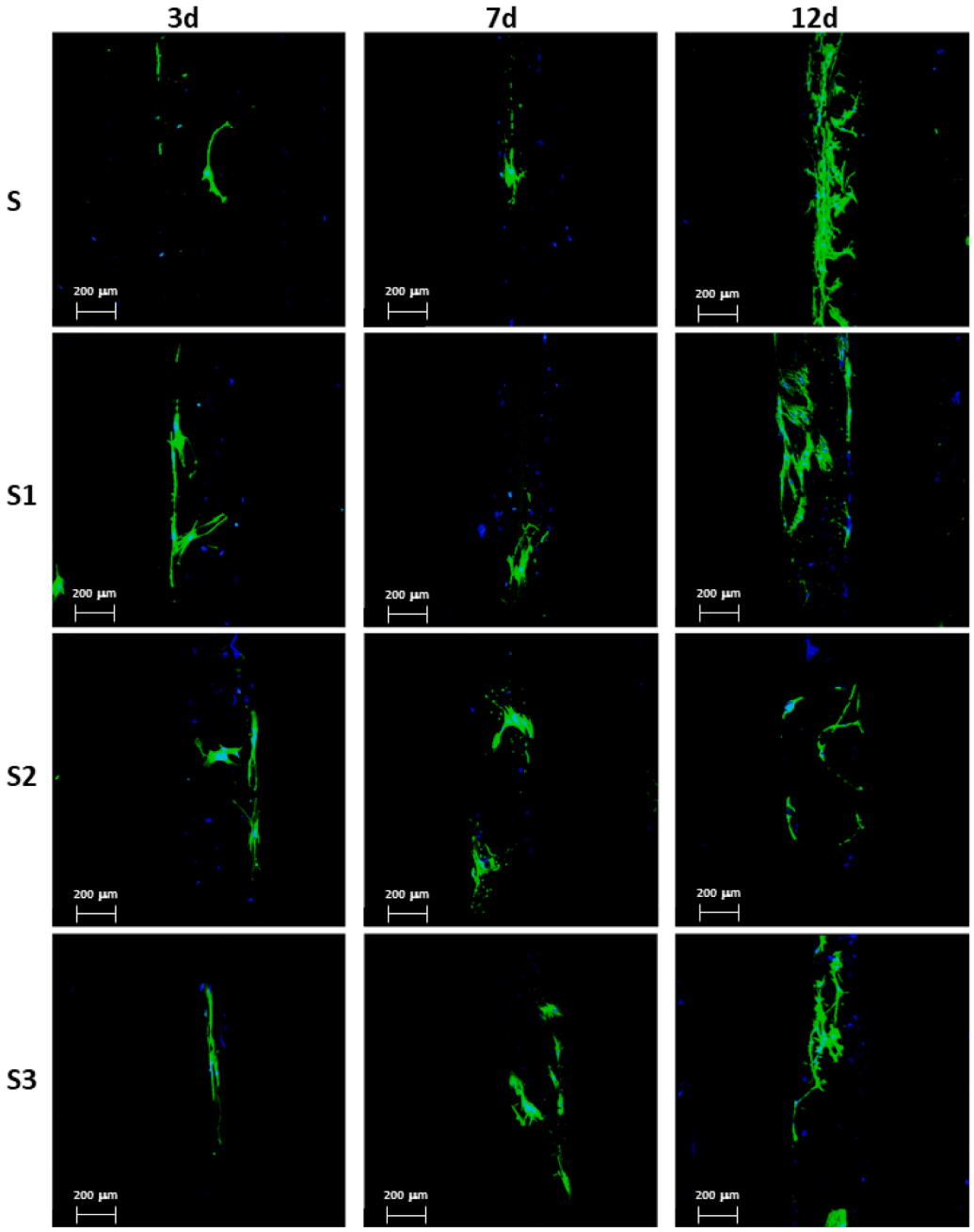

Fig. 14. Confocal micrographs of PCL-based scaffolds after 3, 7 and 12 days of cell culture. Samples were stained for actin with phalloidin (green) and nuclei with DAPI (blue). Scale bar is 200 µm. (For interpretation of the references to colour in this figure legend, the reader is referred to the web version of this article.)

shark skinning) that could negatively affect the printing process and, as reported in Table 1, the diameter values were suitable for printing (values in the range between 2.65 ± 0.09 and 2.83 ± 0.05 mm).

To investigate the homogeneity of the developed polymeric filaments, NMR analysis was conducted on two different fragments sampled at the first and at the last part of the extruded filament Fil3 (Fig. 1) in DMF-d7. PLA/PCL ratio was calculated by comparing the integral of the signal at 5.27 ppm, attributed to PLA –CH group, with the integral of the signal at 2.35 ppm, assigned to the α-protons adjacent to carbonyl group of PCL. Moreover, water content was estimated by comparing the integral of the signal at 3.47 ppm, attributed to water in form of HDO with the integral of the signal at 2.35 ppm of PCL. Since the values obtained from the analysis of the two filament fragments were almost the same (21.0 and 21.6 for the first and the last extruded part of Fil3, respectively), it was assumed that INU-PLA was uniformly distributed in the blend. In addition, the various parts of the filament had the same residual moisture content and no degradation peaks of PCL and PLA were detected, confirming that the extrusion process via HME did not cause any chemical alterations to the material.

Similarly, ^{1}H NMR spectra were recorded for Fil3$_{I}$ in DMF-d7 and D_2O after extraction procedure to isolate signals for PCL and INU respectively. In this case a certain degree of heterogenicity was found; the ratio of the absolute intensity of the signal of inulin (signals in the range 4.32–4.19 ppm, attributed to inulin –OH group) and PCL (signals in the range 2.80–2.20 ppm, assigned to the α-protons adjacent to carbonyl group of PCL) were equal to 99.2 and 104.0 for the first and at the last extruded part of the control filament, respectively.

To gain further information on the blend chemical stability after filament processing and to verify possible interactions between components, filament samples were analyzed by FT-IR (Figure S4). The

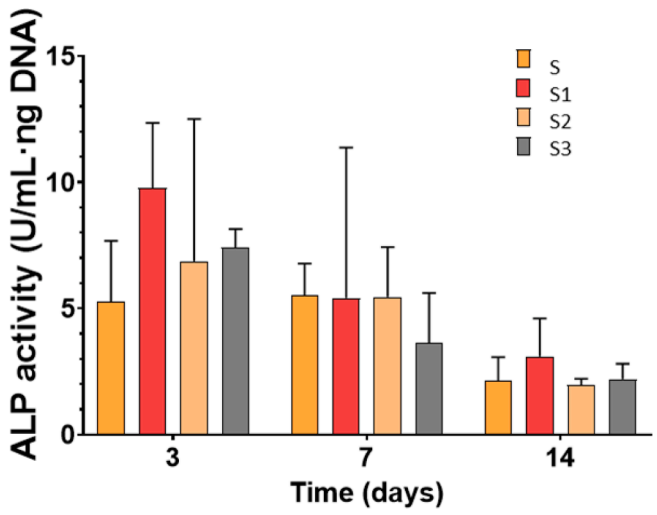

Fig. 15. ALP activity of the PCL-based scaffolds at 3, 7 and 14 days of culture. Data are expressed as mean ± SD.

infrared spectrum of the blended polymeric filaments (PCL/INU-PLA) showed the absorption peaks characteristic of PCL suggesting no chemical alteration after HME. Moreover, no characteristic peak of the INU-PLA copolymer, such as O–H stretching vibration of inulin backbone (3330 cm^{-1}) or absorption band from the carbonyl group of PLA at 1748–1749 cm^{-1} (Sardo et al., 2022) was found. This may be due to the presence of small concentrations of INU-PLA uniformly dispersed within the blend.

Given the direct impact of material surface wettability on cell-material interactions, static water contact angle measurements were conducted (Figure S5). As INU-PLA content increased a statistically significant decrease of contact angle occurred compared to PCL alone. In particular, the contact angle decreased from ~ 83° for PCL, value in agreement with literature data (Huang et al., 2017), to ~ 70° for Fil3, the blend with the highest INU-PLA copolymer content. Therefore, the hydrophilic nature of INU-PLA was communicated to the final polymeric material. Interestingly, INU-PLA copolymer increased PCL wettability even in the low weight percentages tested (2.5, 5.0 and 10.0%), while other blending additives, such as bioceramics, require for this same purpose higher proportions, ranging from 10 to 40% (Dávila et al., 2016). Differently from PCL/INU-PLA blends, neither $Fil3_I$ nor $Fil3_{I+P}$ showed a significant change in the wettability compared to raw PCL. This finding may be due to an irregular distribution of each component (INU and PLA) in the blends.

DSC experiments were conducted to gain an insight into the influence of INU-PLA content on blend processability and the behavior of PCL/INU-PLA filaments (Fig. 2). PCL thermogram recorded during cooling was characterized by a crystallization event in the 24–33 °C range (peak at 30.19 °C) (Fig. 2-a). During the heating cycle, a melting process was observed in the 54–60 °C range (peak at 56.64 °C) (Fig. 2-b). Similar thermal events were observed for all hybrid filaments. The glass transition of INU-PLA also occurred at about 54 °C and, therefore, it was overlapped by the melting peak of the PCL. Nevertheless, the presence of INU-PLA within the blend was confirmed by an endothermic event at about 350 °C, more pronounced for the blend with the highest INU-PLA content and attributable to its degradation (Sardo et al., 2022).

Main thermal parameters evaluated from DSC curves are summarized in Table S1. The addition of INU-PLA to PCL (at all the tested proportions) did not affect neither PCL crystallization nor melting behavior. The thermal investigation conducted on the developed PCL/INU-PLA filaments was helpful to set the process parameters of the next step, namely 3D printing via FFF of bone scaffolds.

3.2. Scaffold additive manufacturing via FFF

The main steps involved in the 3DP process were: 1) the design of the digital model through software CAD, 2) the slicing of the STL structure via CAM software, and 3) the printing of three-dimensional scaffolds accurately matching the initially designed models (Fig. 3). The slicing parameters were selected to fit specific technical requirements necessary for scaffold application in bone tissue engineering (BTE) (e.g., pore size 200–600 μm (Murphy et al., 2010), porosity 50–80%, (Abbasi et al., 2020), and then refined based on printing performances in a given printer configuration.

During preliminary experiments, 3DP operative conditions were set accordingly thermal properties of the developed INU-PLA incorporating PCL filaments. Particularly, printing temperature was maintained in the range 70–100 °C. To guarantee the uniform melting of the polymeric filament within the heated chamber of the nozzle (Ø 0.40 mm) and avoid a discontinuous printing phase with the following possible altered fiber deposition, the lowest printing temperature was fixed at least 10 °C above the melting temperature of the material (T_m around 57 °C; minimal T_{print} 70 °C) (Zhao et al., 2020). Instead, the highest printing temperature value never exceeded 100 °C to avoid slow solidification of each printed layer, which may cause partial collapse of the printed structure. The optimal printing temperature of all the processed filaments resulted to be 85 °C. The print speed was set at 5 mm/s and the speed-while-traveling was set at 250 mm/s. Also the building plate temperature was optimized and finally set at 40 °C to enhance the adhesion of the first layer on the plate and to let the layers partially melting together in the Z dimension.

The refined slicing as well as the printing parameters allowed an adequate print of all the developed filaments, with good layer adhesion in the printed object, dimensional accuracy as compared to the starting digital model and, thus, high resolution (Table 2). Printing of each scaffold took only 4 min.

As reported in Table 2, among the hybrid produced scaffolds (S1, S2 and S3), there were no significant differences in terms of weight, diameter, thickness, and porosity. In particular, dimensional as well as porosity values were very close to those programmed by the software (i.e., 10 mm diameter, 5 mm thickness, and 62% porosity calculated as 1-infill (Buj-Corral et al., 2019)) confirming the high reproducibility of the 3D printed scaffolds.

3.3. 3D architecture and surface topography

As well known, in a layer-by-layer construction process, the controllability of strut diameter is a key aspect. The struts determine pore size, macro-porosity, and tortuosity of the final scaffold (Botchwey et al., 2003; Jeon and Kim, 2012) influencing both mechanical properties (e.g., Youngs modulus and yield stress (Sabree et al., 2015) and activity of the seeded cells such as initial cell attachment, cell migration, cell growth, modulation of phenotypic differentiation, and responses to extracellular signals (Denchai et al., 2018). Therefore, in this work a detailed SEM analysis was conducted to investigate scaffold 3D architecture. The analysis of the micrographs highlighted for all scaffolds a well-defined internal structure made of 0.35–0.40 mm struts forming 0.6 mm horizontal square pores. The horizontal layers of struts were vertically deposited in 0.35 mm superimposition increments (Fig. 3-c and S6). Strut diameter and pore size values obtained by SEM analysis perfectly matched with those initially designed.

Scaffold surface was investigated by UHR-SEM. Scaffolds of PCL (S) had strut surface smoother than those of PCL/INU-PLA. Qualitatively, the higher the INU-PLA graft polymer content within the PCL matrix, the higher the roughness of the strut surface (Fig. 4). This trend was confirmed by surface roughness analysis conducted using ImageJ plug-in SurfCharJ 1 q, which gave the following values of Rq: 13.58 ± 0.95 for S, 18.74 ± 1.48 for S1, 23.34 ± 1.35 for S2 and 30.15 ± 1.90 for S3. Also the Ra parameter was found to be significantly lower for S scaffolds

(10.70 ± 0.69) as compared to those of S1 (14.63 ± 1.14), S2 (17.83 ± 0.89), and S3 (22.69 ± 1.40) (Fig. 5).

The high surface roughness recorded for S3 can be correlated with the presence on scaffolds surface of a higher number of crystalline structures having a peculiar morphology. A detailed topographical analysis conducted via SEM revealed a rough surface completely covered by a high number of crystals with a spherulitic morphology typical of PCL when crystallizes under specific environments (Michell and Mueller, 2016). As reported in literature (Yu et al., 2017), crystalline or semicrystalline polymers, upon melt-crystallization from molten liquids, can show different crystallization kinetics, crystalline structure, and morphology from the bulk and this usually happens when they are in confined systems such as miscible polymer blends (Seraji and Guo, 2020), block copolymers (Seraji and Guo, 2020) or thin films (Liu and Chen, 2010). Based on literature analysis, INU-PLA could be able to induce significant spatial confinement effects towards PCL during the crystallization phase that occurred during the cooling of the printed melt fibers (diameter 0.35–0.40 mm). Such environment affected nucleation and led to a dendritic-like lamellae assembly of PCL. As clearly highlighted by SEM analysis, the peculiar crystal spherulitic morphology was more frequently detected on the surface of S3, i.e. the scaffolds produced blending PCL with the highest INU-PLA amount. For S3, a uniform surface distribution of edge-on lamellae with branches on both sides of the stems was observed (Fig. 6-b,c). Moreover, SEM imaging of strut cross-sections (Fig. 6-e) reveals the uniform presence of such kind of spherulitic structures (dendritic pattern) in the overall fiber volume, suggesting a PCL crystallization by homogeneous nucleation.

The presence of spherulitic crystals in S3 evidenced by SEM analysis did not affect the overall crystallinity of such system compared to the starting filament (Table 3). In fact, for all scaffolds the crystallinity values were close to 49%. The DSC curves of the 3D printed scaffolds (Fig. 7) did not show significant differences with respect to those of the starting filaments (Fig. 2), confirming that the printing process had no particular influence on the thermal properties of the final material.

3.4. Mechanical properties

Mechanical performance of FFF-3D printed scaffolds were assessed by recording the stress–strain curves during compression tests (Figure S7). PCL scaffolds showed a Young's modulus of 34.84 ± 2.37 MPa and a compressive strength of 4.88 ± 0.32 MPa, values in agreement with literature data referred to PCL scaffolds with similar porosity (Hutmacher et al., 2001), and compatible with the range of human trabecular bone (Young's modulus from 1 to 5000 MPa and compressive strength from 0.1 to 27.3 MPa) (Eshraghi and Das, 2010). Interestingly, all the developed PCL/INU-PLA scaffolds exhibited a mechanical behavior very close to those of PCL alone, with values of Young's modulus and compressive strength in the range 31–36 MPa and 4.20–5.28 MPa, respectively. Such findings suggest that the blending of PCL with INU-PLA copolymer does not negatively affect the mechanical performances of the resulting 3D printed scaffolds compared to those based only on PCL. No significant change in the mechanical properties of the scaffolds was detected after their 90-day incubation in PBS.

3.5. Swelling ability

The swelling ability of a scaffold is directly related to the hydrophilicity of the starting biomaterial (Zimmerling et al., 2021) and affects absorption of body fluids, cell attachment, as well as transfer of nutrients and metabolites within the scaffold after its implantation (Kim and Kim, 2013).

To study the influence of material composition on swelling performances, 3D printed scaffolds were incubated in PBS at 37 °C, and changes in mass (measured as percentage of fluid uptake) over time (until 21 days) and in mean strut width after 48 h were monitored. Scaffolds produced with the lowest INU-PLA content (S1) exhibited a swelling profile almost overlapping with that of PCL scaffold (S) (Fig. 8-a), with fluid uptake of approx. 6.5% without significant differences until the third day of incubation. Differently, increasing INU-PLA amount in the starting biomaterial, swelling ability of the resulting scaffolds increased; fluid uptake percentages for both S2 and S3 were higher than that of PCL scaffold (S) and the increase was statistically significant at all the analyzed time points.

The percentage increase in strut width after 48 h of incubation in PBS was also higher for scaffolds of the series PCL/INU-PLA than those of PCL scaffold (5.25% for S1, 7.24% for S2 and 6.93% for S3 versus 3.56% for S) (Fig. 8-b).

Such results confirm the good correlation between INU-PLA content within the blend and the enhancement of the swelling ability of the resulting 3D printed scaffolds as a consequence of the increased wettability/hydrophilicity of the starting biomaterial processed.

3.6. Degradation profiles

In the design of implantable scaffolds for BTE, degradation profile is a critical factor, as the scaffold degradation rate should match the rate of new tissue formation. Aliphatic polyesters biodegrade mainly through hydrolysis under physiological conditions (Woodard and Grunlan, 2018). Specifically, PCL hydrolytic degradation produces caproic acid, that is a non-toxic metabolite (Kweon et al., 2003). Main influencing factors are size (molecular weight), crystallinity, and hydrophilicity of the polymer, as well as temperature and pH of the nearby environment (Kim et al., 2012).

To verify the effect of PCL hybridization with INU-PLA on scaffold biodegradation, 3D printed scaffolds were incubated in PBS at 37 °C for 180 days (6 months). Variations of weight-average molecular weight (M_w), number-average molecular weight (M_n), polydispersity index (PDI) and weight (mass loss %) were evaluated (Fig. 9).

After 180 days of incubation in PBS, the weight loss was about 3% for both S1 and S2, and reached 5% for S3 scaffolds. The molecular weight underwent a slight decrease (from about 101 kDa to 80 kDa), while the polydispersity index (PDI = M_w/M_n) remained almost unchanged over time (1.43–1.54) for all scaffolds.

As hydrolytic degradation was slow, degradation studies under accelerated conditions were also carried out. As reported in literature, chemical or enzymatic methods, may be useful to study the effects of material filler, in our case INU-PLA, on the degradation profile, in a reasonably short time (Vyas et al., 2021). Scaffolds were incubated for 4 days (96 h) in a solution containing PBS and Amano Lipase from *Pseudomonas cepacia*, and weight loss as well as morphological and structural changes were evaluated every day. As shown in Fig. 10-a, the mass variations for the tested scaffolds become to be relevant after 2 days ($t_{48\ h}$) of incubation. At the end of the experiment ($t_{96\ h}$), scaffolds of the series S1 lost about 80% of the initial mass; in fact, the graph showed a remaining mass equal to 20%, value very close to that recorded for the PCL scaffolds (S). A more pronounced enzymatic degradation was observed for both S2 and S3. At $t_{96\ h}$, the remaining mass of such scaffolds was approx. 10%.

For all scaffolds tested, a rapid and significant structure alteration was observed over time. The surface of the fibers progressively become rougher, their diameter decreases, resulting in an increase in pore size (see SEM micrographs reported in Fig. 10-b and Figure S8).

During the enzymatic degradation experiments, the scaffold fibers begin to detach from each other, altering each layer and flaking the scaffold. Such modifications were more pronounced as the concentration of INU-PLA within the PCL matrix increased. In fact, at $t_{96\ h}$, both S2 and S3 completely lose their structural integrity, and only pieces remained (Figure S9). Since lipases only degrade PCL, this effect could probably be due to the progressive release of the graft copolymer embedded within the PCL matrix. Thus, as INU-PLA is released, this increases the surface area available for the enzymatic degradation within the matrix of PCL, increasing the rate of degradation. In addition,

the higher the graft copolymer content within the blend, the lower the amount of PCL, resulting in an increased scaffold degradability.

3.7. In vitro biological evaluation

As scaffolds will be, in vivo, into direct contact with blood, hemolysis test represent a valuable preliminary tool to evaluate in vitro their biocompatibility (Shao et al., 2016). The scaffolds showed hemolysis percentages (Fig. 11) well below the maximum allowed value of 5%, according the ASTM F765-00 (Asif et al., 2014; ASTM, 2000). All PCL/INU-PLA scaffolds, regardless of INU-PLA amount within the blend, exhibited hemolysis values always around 0.5%, and thus the same hemocompatibility of PCL scaffolds.

In vitro cytotoxicity of 3D printed scaffolds was preliminary evaluated against human fibroblast MRC-5 cells, using lactate dehydrogenase (LDH) cytotoxicity assay.

The LDH release after 48 h of direct contact with cells revealed adequate cytocompatibility. In fact, as reported in Fig. 12, the recorded percentages of relative cytotoxicity were 10–17%, values falling within the range of non-toxicity according to ISO10993-5:2009 (ISO, 2009; Jung et al., 2019).

As well known, mesenchymal stem cells are a more relevant cell line for the evaluation of cell viability on scaffolds intended for bone tissue engineering than fibroblasts since they are a key cell line during the regeneration process in the bone. Therefore, the biological evaluation was conducted using human adipose-derived mesenchymal stem cells. By using the CCK-8 assay we observed that cell viability was not affected by the composition of the scaffolds (Fig. 13). All conditions presented cell viability close to 100%, compared to the controls.

Confocal microscopy images showed that cells covered the surface of the fibers, regardless of the composition of the scaffolds, as depicted in Fig. 14. After 12 days, all scaffolds exhibited an increased cell density. The effect of scaffolds composition on density of cells on the surface of the fibers during the evaluated culture time was negligible. At each timepoint, cells displayed an elongated cytoplasm, indicative of cell spreading and migration, similar to what was previously observed in 3D printed scaffolds with comparable polyester composition (Kim et al., 2021).

To evaluate the early osteogenic differentiation of hMSCs, ALP activity was measured on days 3, 7 and 14 of cell culture. ALP activity showed no differences in the osteogenic differentiation of hMSCs (Fig. 15). ALP activity was higher at earlier timepoints (3 and 7 days). As observed for all conditions, alkaline phosphatase is significantly expressed by osteogenic cells in the first days after osteodifferentiation. The obtained results confirmed that no condition led to a time delay in the enzymatic activity of ALP, which could be attributed to a decreased osteogenic ability of the scaffolds. Our results are in agreement with previous studies reporting a significant upregulation of ALP at early culture times (3 and 7 days) (Arab-Ahmadi et al., 2021; Ebrahimi et al., 2022; Marino et al., 2010). Moreover, the selected pore size of the scaffolds may also drove a substantial osteoconductive effect, as previously reported (Florencio-Silva et al., 2015; Shi et al., 2021).

In summary, the in vitro results obtained for the 3D printed PCL/INU-PLA scaffolds suggest the potential of such hybrid materials to produce implantable scaffolds for bone tissue engineering applications. Specifically, the results encourage further in vitro studies on hMSCs to better validate the developed systems, and pave the way for the potential use of these systems in BTE.

4. Conclusions

PCL/INU-PLA hybrid biomaterial obtained blending PCL with the recently synthetized amphiphilic graft copolymer inulin-g-poly(D,L) lactide (INU-PLA) exhibited excellent properties to be transformed in filaments for FFF 3D printing. The hybrid filaments showed good component miscibility, and consequently high homogeneity, thermal properties suitable for 3D printing, and improved surface wettability compared to PCL alone thanks to a more hydrophilic nature of the INU-PLA blending copolymer.

The final scaffolds (i.e., S1, S2, and S3) may be fabricate by 3D printing with a predictable, customizable, and reproducible internal architecture. Scaffolds retain the good mechanical properties as well as the biocompatibility of PCL, but show significantly improved surface properties, swelling ability and biodegradation profiles. Relevantly, the inclusion of the graft copolymer INU-PLA within the biomaterial determines an overall enzymatic degradation rate of the scaffold higher as compared to scaffold made of PCL alone. All hybrid scaffolds exhibit both good hemocompatibility and compatibility with human fibroblasts. More importantly, the constructs show high compatibility with hMSCs, as well as good osteogenic activity proved by significant early up-regulation of ALP.

The overall results confirm the validity of the polymeric blending PCL/INU-PLA, as a valid strategy to maintain and benefit from positive features of PCL (mainly biocompatibility, biodegradability, and easy processability via FFF-3DP), while addressing its restraints (i.e. poor wettability/hydrophilicity and slow biodegradation). Our study also confirms the great versatility of FFF-3D printing technique in the production of macroporous scaffolds with controllable and, eventually, on demand modifiable size, porosity, and 3D architecture. Therefore, the PCL/INU-PLA hybrid biomaterial and FFF-3D printing technique, can be considered a successful duo for the development of novel scaffolds for BTE applications.

Funding

This research was funded by MIUR within the project "Centro nazionale di ricerca e sviluppo di terapia genica e farmaci con tecnologia a RNA [CN00000041], MCIN [PID 2020-113881RB-I00/AEI/10.13039/501100011033] Spain, Xunta de Galicia [ED431C 2020/17], and FEDER (Spain).

CRediT authorship contribution statement

Carmela Tommasino: Data curation, Formal analysis, Investigation, Methodology, Writing – original draft. **Giulia Auriemma:** Conceptualization, Data curation, Formal analysis, Methodology, Validation, Writing – original draft, Writing – review & editing. **Carla Sardo:** Conceptualization, Investigation, Methodology, Validation, Writing – review & editing. **Carmen Alvarez-Lorenzo:** Funding acquisition, Methodology, Writing – original draft. **Emilia Garofalo:** Investigation, Methodology. **Silvana Morello:** Data curation, Methodology, Writing – review & editing. **Giovanni Falcone:** Visualization. **Rita P. Aquino:** Funding acquisition, Project administration, Resources, Supervision, Writing - review & editing.

Declaration of Competing Interest

The authors declare they have no known competing financial interests or personal relationships that could have appeared to influence the work reported in this paper.

Data availability

Data will be made available on request.

Acknowledgements

The authors thank Luis Antonio Diaz Gomez (University of Santiago de Compostela) for his excellent technical support during the in vitro assays on hMSCs and Patrizia Picerno for the technical support during the SEM analysis.

Appendix A. Supplementary data

Supplementary data to this article can be found online at https://doi.org/10.1016/j.ijpharm.2023.123093.

References

Abbasi, N., Hamlet, S., Love, R.M., Nguyen, N.-T., 2020. Porous scaffolds for bone regeneration. J. Sci.: Adv. Mater. Devices 5, 1–9.

Alhosseini, S.N., Moztarzadeh, F., Mozafari, M., Asgari, S., Dodel, M., Samadikuchaksaraei, A., Kargozar, S., Jalali, N., 2012. Synthesis and characterization of electrospun polyvinyl alcohol nanofibrous scaffolds modified by blending with chitosan for neural tissue engineering. Int. J. Nanomed. 7, 25.

Arab-Ahmadi, S., Irani, S., Bakhshi, H., Atyabi, F., Ghalandari, B., 2021. Immobilization of carboxymethyl chitosan/laponite on polycaprolactone nanofibers as osteoinductive bone scaffolds. Polym. Adv. Technol. 32, 755–765.

Asif, A., Nazir, R., Riaz, T., Ashraf, N., Zahid, S., Shahid, R., Ur-Rehman, A., Chaudhry, A. A., Ur Rehman, I., 2014. Influence of processing parameters and solid concentration on microstructural properties of gel-casted porous hydroxyapatite. J. Porous Mater. 21, 31–37.

ASTM, F., 2000. 756-00. Standard practice for assessment of hemolytic properties of materials. American Society for Testing and Materials, Philadelphia.

Babaie, E., Bhaduri, S.B., 2018. Fabrication aspects of porous biomaterials in orthopedic applications: A review. ACS Biomater Sci. Eng. 4, 1–39.

Bazgir, M., Zhang, W., Zhang, X., Elies, J., Saeinasab, M., Coates, P., Youseffi, M., Sefat, F., 2021. Degradation and characterisation of electrospun polycaprolactone (PCL) and poly (lactic-co-glycolic acid)(PLGA) scaffolds for vascular tissue engineering. Materials 14, 4773.

Bittner, S.M., Smith, B.T., Diaz-Gomez, L., Hudgins, C.D., Melchiorri, A.J., Scott, D.W., Fisher, J.P., Mikos, A.G., 2019. Fabrication and mechanical characterization of 3D printed vertical uniform and gradient scaffolds for bone and osteochondral tissue engineering. Acta Biomater. 90, 37–48.

Boland, E.D., Wnek, G.E., Simpson, D.G., Pawlowski, K.J., Bowlin, G.L., 2001. Tailoring tissue engineering scaffolds using electrostatic processing techniques: a study of poly (glycolic acid) electrospinning. J. Macromol. Sci. A 38, 1231–1243.

Botchwey, E.A., Dupree, M.A., Pollack, S.R., Levine, E.M., Laurencin, C.T., 2003. Tissue engineered bone: Measurement of nutrient transport in three-dimensional matrices. Journal of Biomedical Materials Research Part A: An Official Journal of The Society for Biomaterials, The Japanese Society for Biomaterials, and The Australian Society for Biomaterials and the Korean Society for Biomaterials 67, 357–367.

Bruyas, A., Lou, F., Stahl, A.M., Gardner, M., Maloney, W., Goodman, S., Yang, Y.P., 2018. Systematic characterization of 3D-printed PCL/β-TCP scaffolds for biomedical devices and bone tissue engineering: Influence of composition and porosity. J. Mater. Res. 33, 1948–1959.

Buj-Corral, I., Bagheri, A., Domínguez-Fernández, A., Casado-López, R., 2019. Influence of infill and nozzle diameter on porosity of FDM printed parts with rectilinear grid pattern. Procedia Manuf. 41, 288–295.

Chinga, G., Johnsen, P.O., Dougherty, R., Berli, E.L., Walter, J., 2007. Quantification of the 3D microstructure of SC surfaces. Journal of Microscopy 227, 254–265.

Chocholata, P., Kulda, V., Babuska, V., 2019. Fabrication of Scaffolds for Bone-Tissue Regeneration. Materials 12, 568.

Dávila, J., Freitas, M., Inforçatti Neto, P., Silveira, Z., Silva, J., d'Ávila, M., 2016. Fabrication of PCL/β-TCP scaffolds by 3D mini-screw extrusion printing. J. Appl. Polym. Sci. 133.

Denchai, A., Tartarini, D., Mele, E., 2018. Cellular response to surface morphology: electrospinning and computational modeling. Front. Bioeng. Biotechnol. 155.

Dwivedi, R., Kumar, S., Pandey, R., Mahajan, A., Nandana, D., Katti, D.S., Mehrotra, D., 2020. Polycaprolactone as biomaterial for bone scaffolds: Review of literature. Journal of oral biology and craniofacial research 10, 381–388.

Ebrahimi, Z., Irani, S., Ardeshirylajimi, A., Seyedjafari, E., 2022. Enhanced osteogenic differentiation of stem cells by 3D printed PCL scaffolds coated with collagen and hydroxyapatite. Sci. Rep. 12, 12359.

Eltom, A., Zhong, G., Muhammad, A., 2019. Scaffold techniques and designs in tissue engineering functions and purposes: a review. Advances in materials science and engineering 2019.

Eshraghi, S., Das, S., 2010. Mechanical and microstructural properties of polycaprolactone scaffolds with one-dimensional, two-dimensional, and three-dimensional orthogonally oriented porous architectures produced by selective laser sintering. Acta Biomater 6, 2467–2476.

Florencio-Silva, R., Sasso, G.R.d.S., Sasso-Cerri, E., Simões, M.J., Cerri, P.S., 2015. Biology of bone tissue: structure, function, and factors that influence bone cells. BioMed research international 2015.

Fu, Q., Saiz, E., Rahaman, M.N., Tomsia, A.P., 2011. Bioactive glass scaffolds for bone tissue engineering: state of the art and future perspectives. Mater Sci Eng C Mater Biol Appl 31, 1245–1256.

Fulmer, G.R., Miller, A.J., Sherden, N.H., Gottlieb, H.E., Nudelman, A., Stoltz, B.M., Bercaw, J.E., Goldberg, K.I., 2010. NMR chemical shifts of trace impurities: common laboratory solvents, organics, and gases in deuterated solvents relevant to the organometallic chemist. Organometallics 29, 2176–2179.

Gadelmawla, E., Koura, M.M., Maksoud, T.M., Elewa, I.M., Soliman, H., 2002. Roughness parameters. J. Mater. Process. Technol. 123, 133–145.

Grabowski, P., 2015. Physiology of bone. Calcium and Bone Disorders in Children and Adolescents 28, 33–55.

Hamlehkhan, A., Mozafari, M., Nezafati, N., Azami, M., Samadikuchaksaraei, A., 2012. Novel bioactive poly (ε-caprolactone)-gelatin-hydroxyapatite nanocomposite scaffolds for bone regeneration. Key Engineering Materials. Trans Tech Publ 909–915.

Huang, A., Jiang, Y., Napiwocki, B., Mi, H., Peng, X., Turng, L.-S., 2017. Fabrication of poly (ε-caprolactone) tissue engineering scaffolds with fibrillated and interconnected pores utilizing microcellular injection molding and polymer leaching. RSC Adv. 7, 43432–43444.

Huhtamäki, T., Tian, X., Korhonen, J.T., Ras, R.H., 2018. Surface-wetting characterization using contact-angle measurements. Nat. Protoc. 13, 1521–1538.

Hutmacher, D.W., Schantz, T., Zein, I., Ng, K.W., Teoh, S.H., Tan, K.C., 2001. Mechanical properties and cell cultural response of polycaprolactone scaffolds designed and fabricated via fused deposition modeling. J Biomed Mater Res 55, 203–216.

Iso, 2009. Biological Evaluation of Medical Devices—Part 5: Tests for in Vitro Cytotoxicity, ISO 10993–5: 2009. ISO Geneva, Switzerland.

Jeon, H., Kim, G.H., 2012. Effect of the internal microstructure in rapid-prototyped polycaprolactone scaffolds on physical and cellular properties for bone tissue regeneration. Appl. Phys. A 108, 901–909.

Jung, O., Smeets, R., Hartjen, P., Schnettler, R., Feyerabend, F., Klein, M., Wegner, N., Walther, F., Stangier, D., Henningsen, A., Rendenbach, C., Heiland, M., Barbeck, M., Kopp, A., 2019. Improved In Vitro Test Procedure for Full Assessment of the Cytocompatibility of Degradable Magnesium Based on ISO 10993-5/-12. Int J Mol Sci 20.

Kalirajan, C., Behera, H., Selvaraj, V., Palanisamy, T., 2022. In vitro probing of oxidized inulin cross-linked collagen-ZrO2 hybrid scaffolds for tissue engineering applications. Carbohydr. Polym. 289, 119458.

Kim, J.Y., Ahn, G., Kim, C., Lee, J.S., Lee, I.G., An, S.H., Yun, W.S., Kim, S.Y., Shim, J.H., 2018. Synergistic Effects of Beta Tri-Calcium Phosphate and Porcine-Derived Decellularized Bone Extracellular Matrix in 3D-Printed Polycaprolactone Scaffold on Bone Regeneration. Macromol Biosci 18, e1800025.

Kim, J.-W., Han, Y.-S., Lee, H.-M., Kim, J.-K., Kim, Y.-J., 2021. Effect of morphological characteristics and biomineralization of 3D-printed gelatin/hyaluronic acid/hydroxyapatite composite scaffolds on bone tissue regeneration. Int. J. Mol. Sci. 22, 6794.

Kim, Y., Kim, G., 2013. Collagen/alginate scaffolds comprising core (PCL)–shell (collagen/alginate) struts for hard tissue regeneration: fabrication, characterisation, and cellular activities. J. Mater. Chem. B 1, 3185–3194.

Kim, Y.B., Kim, G.H., 2015. PCL/alginate composite scaffolds for hard tissue engineering: fabrication, characterization, and cellular activities. ACS Comb. Sci. 17, 87–99.

Kim, Y.-J., Park, M.R., Kim, M.S., Kwon, O.H., 2012. Polyphenol-loaded polycaprolactone nanofibers for effective growth inhibition of human cancer cells. Mater. Chem. Phys. 133, 674–680.

Kumar, G., Waters, M.S., Farooque, T.M., Young, M.F., Simon Jr., C.G., 2012. Freeform fabricated scaffolds with roughened struts that enhance both stem cell proliferation and differentiation by controlling cell shape. Biomaterials 33, 4022–4030.

Kutikov, A.B., Gurijala, A., Song, J., 2015. Rapid prototyping amphiphilic polymer/hydroxyapatite composite scaffolds with hydration-induced self-fixation behavior. Tissue Eng Part C Methods 21, 229–241.

Kweon, D.-K., Song, S.-B., Park, Y.-Y., 2003. Preparation of water-soluble chitosan/heparin complex and its application as wound healing accelerator. Biomaterials 24, 1595–1601.

Lam, C.X., Hutmacher, D.W., Schantz, J.T., Woodruff, M.A., Teoh, S.H., 2009. Evaluation of polycaprolactone scaffold degradation for 6 months in vitro and in vivo. Journal of Biomedical Materials Research Part A: An Official Journal of The Society for Biomaterials, The Japanese Society for Biomaterials, and The Australian Society for Biomaterials and the Korean Society for Biomaterials 90, 906–919.

Li, W.J., Laurencin, C.T., Caterson, E.J., Tuan, R.S., Ko, F.K., 2002. Electrospun nanofibrous structure: a novel scaffold for tissue engineering. Journal of Biomedical Materials Research: An Official Journal of The Society for Biomaterials, The Japanese Society for Biomaterials, and The Australian Society for Biomaterials and the Korean Society for Biomaterials 60, 613–621.

Liu, Y.-X., Chen, E.-Q., 2010. Polymer crystallization of ultrathin films on solid substrates. Coord. Chem. Rev. 254, 1011–1037.

Loh, Q.L., Choong, C., 2013. Three-dimensional scaffolds for tissue engineering applications: role of porosity and pore size.

Malberg, S., Höglund, A., Albertsson, A.-C., 2011. Macromolecular design of aliphatic polyesters with maintained mechanical properties and a rapid, customized degradation profile. Biomacromolecules 12, 2382–2388.

Marino, G., Rosso, F., Cafiero, G., Tortora, C., Moraci, M., Barbarisi, M., Barbarisi, A., 2010. β-Tricalcium phosphate 3D scaffold promote alone osteogenic differentiation of human adipose stem cells: in vitro study. J. Mater. Sci. - Mater. Med. 21, 353–363.

Mensink, M.A., Frijlink, H.W., van der Voort Maarschalk, K., Hinrichs, W.L., 2015. Inulin, a flexible oligosaccharide I: Review of its physicochemical characteristics. Carbohydr. Polym. 130, 405–419.

Meyer, D., Stasse-Wolthuis, M., 2006. Inulin and bone health. Current Topics in Nutraceutical Research 4, 211–225.

Mi, H.-Y., Jing, X., Peng, J., Salick, M.R., Peng, X.-F., Turng, L.-S., 2014. Poly (ε-caprolactone)(PCL)/cellulose nano-crystal (CNC) nanocomposites and foams. Cellul. 21, 2727–2741.

Michell, R.M., Mueller, A.J., 2016. Confined crystallization of polymeric materials. Prog. Polym. Sci. 54, 183–213.

Montero, J., Becerro, A., Pardal-Peláez, B., Quispe-López, N., Blanco, J.-F., Gómez-Polo, C., 2021. Main 3D Manufacturing Techniques for Customized Bone Substitutes. A Systematic Review. Materials 14, 2524.

Murphy, C.M., Haugh, M.G., O'brien, F.J.,, 2010. The effect of mean pore size on cell attachment, proliferation and migration in collagen–glycosaminoglycan scaffolds for bone tissue engineering. Biomaterials 31, 461–466.
Nzeusseu, A., Dienst, D., Haufroid, V., Depresseux, G., Devogelaer, J.-P., Manicourt, D.-H., 2006. Inulin and fructo-oligosaccharides differ in their ability to enhance the density of cancellous and cortical bone in the axial and peripheral skeleton of growing rats. Bone 38, 394–399.
Sabree, I., Gough, J.E., Derby, B., 2015. Mechanical properties of porous ceramic scaffolds: influence of internal dimensions. Ceram. Int. 41, 8425–8432.
Sardo, C., Craparo, E.F., Porsio, B., Giammona, G., Cavallaro, G., 2016. Improvements in rational design strategies of inulin derivative polycation for siRNA delivery. Biomacromolecules 17, 2352–2366.
Sardo, C., Mencherini, T., Tommasino, C., Esposito, T., Russo, P., Del Gaudio, P., Aquino, R.P., 2022. Inulin-g-poly-D, L-lactide, a Sustainable Amphiphilic Copolymer for Nano-Therapeutics. Drug Deliv. Transl. Res. 12, 1974–1990.
Schätzlein, E., Kicker, C., Söhling, N., Ritz, U., Neijhoft, J., Henrich, D., Frank, J., Marzi, I., Blaeser, A., 2022. 3D-Printed PLA-Bioglass Scaffolds with Controllable Calcium Release and MSC Adhesion for Bone Tissue Engineering. Polymers 14, 2389.
Seraji, S.M., Guo, Q., 2020. Polymorphism and crystallization in poly (vinylidene fluoride)/poly (ϵ-caprolactone)–block–poly (dimethylsiloxane)–block–poly (ϵ-caprolactone) blends. Polym. Int. 69, 173–183.
Shahbazi, M., Jäger, H., Ettelaie, R., Chen, J., 2021. Construction of 3D printed reduced-fat meat analogue by emulsion gels. Part I: Flow behavior, thixotropic feature, and network structure of soy protein-based inks. Food Hydrocoll. 120, 106967.
Shao, W., He, J., Sang, F., Wang, Q., Chen, L., Cui, S., Ding, B., 2016. Enhanced bone formation in electrospun poly (l-lactic-co-glycolic acid)–tussah silk fibroin ultrafine nanofiber scaffolds incorporated with graphene oxide. Mater. Sci. Eng. C 62, 823–834.
Shi, F., Xiao, D., Zhang, C., Zhi, W., Liu, Y., Weng, J., 2021. The effect of macropore size of hydroxyapatite scaffold on the osteogenic differentiation of bone mesenchymal stem cells under perfusion culture. Regener. Biomater. 8, rbab050.
Tripodo, G., Mandracchia, D., 2019. Inulin as a multifaceted (active) substance and its chemical functionalization: From plant extraction to applications in pharmacy, cosmetics and food. Eur. J. Pharm. Biopharm. 141, 21–36.
Van Hoorick, J., Delaey, J., Vercammen, H., Van Erps, J., Thienpont, H., Dubruel, P., Zakaria, N., Koppen, C., Van Vlierberghe, S., Van den Bogerd, B., 2020. Designer descemet membranes containing PDLLA and functionalized gelatins as corneal endothelial scaffold. Adv. Healthc. Mater. 9, 2000760.
Verdú, E., Labrador, R.O., Rodríguez, F.J., Ceballos, D., Forés, J., Navarro, X., 2002. Alignment of collagen and laminin-containing gels improve nerve regeneration within silicone tubes. Restor. Neurol. Neurosci. 20, 169–180.
Vyas, C., Zhang, J., Øvrebø, Ø., Huang, B., Roberts, I., Setty, M., Allardyce, B., Haugen, H., Rajkhowa, R., Bartolo, P., 2021. 3D printing of silk microparticle reinforced polycaprolactone scaffolds for tissue engineering applications. Mater. Sci. Eng. C 118, 111433.
Wang, X., Molino, B.Z., Pitkänen, S., Ojansivu, M., Xu, C., Hannula, M., Hyttinen, J., Miettinen, S., Hupa, L., Wallace, G., 2019. 3D Scaffolds of Polycaprolactone/Copper-Doped Bioactive Glass: Architecture Engineering with Additive Manufacturing and Cellular Assessments in a Coculture of Bone Marrow Stem Cells and Endothelial Cells. ACS Biomater Sci. Eng. 5, 4496–4510.
Wang, L., Wang, C., Zhou, L., Bi, Z., Shi, M., Wang, D., Li, Q., 2021a. Fabrication of a novel Three-Dimensional porous PCL/PLA tissue engineering scaffold with high connectivity for endothelial cell migration. Eur. Polym. J. 161, 110834.
Wang, W., Zhang, B., Li, M., Li, J., Zhang, C., Han, Y., Wang, L., Wang, K., Zhou, C., Liu, L., Fan, Y., Zhang, X., 2021b. 3D printing of PLA/n-HA composite scaffolds with customized mechanical properties and biological functions for bone tissue engineering. Compos. B Eng. 224, 109192.
Wen, Y., Che, Q.T., Kim, H.W., Park, H.J., 2021. Potato starch altered the rheological, printing, and melting properties of 3D-printable fat analogs based on inulin emulsion-filled gels. Carbohydr. Polym. 269, 118285.
Woodard, L.N., Grunlan, M.A., 2018. Hydrolytic Degradation and Erosion of Polyester Biomaterials. ACS Macro Lett 7, 976–982.
Wu, S., Zellnitz, S., Mercuri, A., Salar-Behzadi, S., Bresciani, M., Fröhlich, E., 2016. An in vitro and in silico study of the impact of engineered surface modifications on drug detachment from model carriers. Int J Pharm 513, 109–117.
Xiang, P., Wang, S.-S., He, M., Han, Y.-H., Zhou, Z.-H., Chen, D.-L., Li, M., Ma, L.Q., 2018. The in vitro and in vivo biocompatibility evaluation of electrospun recombinant spider silk protein/PCL/gelatin for small caliber vascular tissue engineering scaffolds. Colloids Surf. B Biointerfaces 163, 19–28.
Yan, C., Huang, D., Shen, X., Qin, N., Jiang, K., Zhang, D., Zhang, Q., 2019. Identification and characterization of a polysaccharide from the roots of Morinda officinalis, as an inducer of bone formation by up-regulation of target gene expression. Int. J. Biol. Macromol. 133, 446–456.
Yu, C., Xie, Q., Bao, Y., Shan, G., Pan, P., 2017. Crystalline and spherulitic morphology of polymers crystallized in confined systems. Crystals 7, 147.
Zhang, Y., Liu, X., Zeng, L., Zhang, J., Zuo, J., Zou, J., Ding, J., Chen, X., 2019. Polymer fiber scaffolds for bone and cartilage tissue engineering. Adv. Funct. Mater. 29, 1903279.
Zhao, Y.-Q., Yang, J.-H., Ding, X., Ding, X., Duan, S., Xu, F.-J., 2020. Polycaprolactone/polysaccharide functional composites for low-temperature fused deposition modelling. Bioact. Mater. 5, 185–191.
Zimmerling, A., Yazdanpanah, Z., Cooper, D.M.L., Johnston, J.D., Chen, X., 2021. 3D printing PCL/nHA bone scaffolds: exploring the influence of material synthesis techniques. Biomater Res 25, 3.